Influence of bonding layer on effective electromechanical properties of macro-fiber composites (MFCs)

2014 Smart Mater. Struct. 23 095046

(http://iopscience.iop.org/0964-1726/23/9/095046)

IOP Publishing Smart Materials and Structures
Smart Mater. Struct. **23** (2014) 095046 (19pp) doi:10.1088/0964-1726/23/9/095046

Influence of bonding layer on effective electromechanical properties of macro-fiber composites (MFCs)

S Sreenivasa Prasath and A Arockiarajan

Department of Applied Mechanics, Indian Institute of Technology Madras, Chennai 600 036, India

E-mail: aarajan@iitm.ac.in

Received 2 May 2014
Accepted for publication 14 July 2014
Published 15 August 2014

Abstract

An analytical model based on an equivalent layered approach using iso-field assumptions is proposed to find the effect of bonding layers on the effective properties of macro-fiber composites (MFCs). To account for the interdigitated electrode pattern and geometric (shape and position) properties, a finite element analysis is carried out using the representative volume element (RVE) method. The simulated results based on the proposed analytical and numerical models are compared and validated with the data available from the manufacturer and a mixing rules model available in the literature. Experiments are performed on MFCs under pure electrical loading to measure a few coupling constants and the results are compared with simulated results. A parametric study is conducted to investigate the variations of the overall material behavior of MFCs with respect to bonding layer thickness. The present study examines the influence of bonding the layer on the effective properties of MFCs.

Keywords: d_{31} and d_{33} type MFC, Effective properties, Interphase effects, Equivalent layered approach, Unit cell model

(Some figures may appear in colour only in the online journal)

1. Introduction

Piezoelectric ceramics (PZT) are a class of smart materials often used as sensors and actuators due to their coupled electromechanical behavior [1]. Due to their unique coupling behavior, these materials are very attractive in vibration control, structural health monitoring, energy harvesting, and structural morphing applications [2–4]. Though bulk piezoceramics are extensively used for sensing and actuation applications, they have some limitations such as brittleness and low flexibility, which can cause premature failure; they are difficult to attach to curved surfaces [5]. In order to overcome these limitations, piezoelectric composites were developed [6].

Initially, piezoelectric-fiber composites (PFC) were introduced wherein an active piezoceramic fibrous phase was embedded in a polymeric matrix phase, resulting in increased flexibility and reliability compared with bulk piezoceramics [7]. In PFCs, electrode layers were placed on the top and bottom of the single fiber layer, along with matrix. This configuration generates an electric field along the thickness direction of the PFCs, resulting in transverse (d_{31}) actuation. In order to have longitudinal (d_{33}) actuation, the concept of interdigitated electrodes is introduced along with PFCs, referred to as interdigitated electrode piezoelectric-fiber composites (IDEPFC). These IDEPFCs are also known as active fiber-composites (AFC) [8, 9]. However, in an AFC, the active PZT fibers are in a circular cross section which has limited contact with the flat copper electrode, and the alignment of PZT fibers during the manufacturing process is difficult because they are brittle. To overcome such limitations, NASA developed macro-fiber composites (MFCs), wherein rectangular PZT fibers are embedded in a polymer matrix, referred to as the active layer. This active layer is sandwiched between different protective and electrode layers [10]. The method of MFC fabrication are reported by High and Wilkie [11], who elaborate on the step-by-step procedures for their assembly. The assembly sequence involves the inspection of

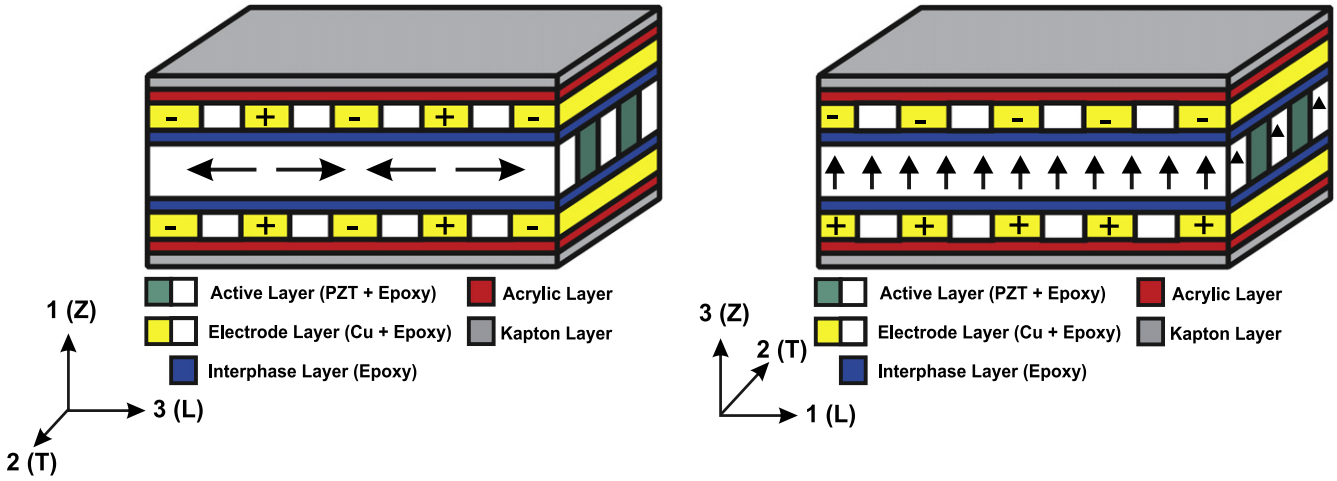

Figure 1. Schematic representation of longitudinal (d_{33}) and transverse (d_{31}) type Macro-Fiber Composite.

the interdigitated electrode film pattern for connectivity, incorporation of epoxy adhesive in both the electroded area and on top of the diced rectangular PZT fibers, and attachment of the electrode layer to the piezoceramic fibers using a vacuum press stack lay-up technique. The thin layer present between the electrode layer and the active layer is called the bonding layer.

To understand the behavior of structural systems equipped with piezocomposites, it is necessary to have comprehensive knowledge of the behavior of piezocomposites. Several attempts have been reported in the literature to predict the effective electromechanical properties of piezocomposites using both analytical and numerical approaches. Park and Kim [12] employed the classical lamination theory and the uniform field model (UFM) to show that the performance of MFCs can be improved by using single crystals instead of polycrystalline piezofibers. A seven-layer shear actuated-fiber composite (SAFC) model was introduced [13], and its effective properties were predicted using a UFM (active layer) and shear deformation lamination theory. Also, a finite-element-based homogenization approach was reported in the literature [14] for shear-actuated d_{15}-type MFCs.

A simple analytical method based on plane stress conditions and assuming a uniform electric field across electrodes was proposed to study the longitudinal and transverse piezoelectric coefficients of d_{31}- and d_{33}-type MFCs and to validate them with both finite element computations and experimental results [15]. To account for curved electric fields across electrodes due to an interdigitated electrode pattern, a finite element periodic homogenization was performed [16]. Also, an attempt has been made to study the effective electromechanical properties of MFC transducers using the asymptotic expansion homogenization (AEH) method, wherein the effect of electrodes were neglected [17]. The directionality of the piezoelectric effect on the piezocomposites was investigated and optimized for layered piezoelectric transducers using analytical mixing rules and a numerical homogenization method [18].

Table 1. Sequence of formulation for homogenization of MFCs using an equivalent layered approach.

Sequence of formulation	$(*)^c$	$(*)^f$	$(*)^m$
I.a	Active layer (V^{act})	PZT	Epoxy
I.b	Electrode layer (V^e)	Copper	Epoxy
II	Homogenized layer (V^{act} & V^i)	Active layer (V^{act})	bonding layer (V^i)
III	Homogenized layer (V^{act}, V^i & V^e)	Homogenized layer (V^{act} & V^i)	Electrode layer (V^e)
IV	Homogenized layer (V^{act}, V^i, V^e & V^a)	Homogenized layer (V^{act}, V^i & V^e)	Acrylic layer (V^a)
V	Homogenized layer (V^{act}, V^i, V^e, V^a & V^k)	Homogenized layer (V^{act}, V^i, V^e & V^a)	Kapton layer (V^k)

As far as the authors know, previous models of MFCs reported in the literature have not considered the effect of the bonding layer for homogenization. However, the bonding layer between the electrode and active layers may have an effect on coupling and electrical constants because the generated electric field in the electrode layer has to pass through the bonding layer to the active layer. The bonding layer is a thin layer present between fiber and matrix of fiber reinforced composites [19]. The bonding layer is formed by adding a protective coating to ensure good adhesion between the reinforcement and the matrix. Although the dimensions of the bonding layer are small, the bonding

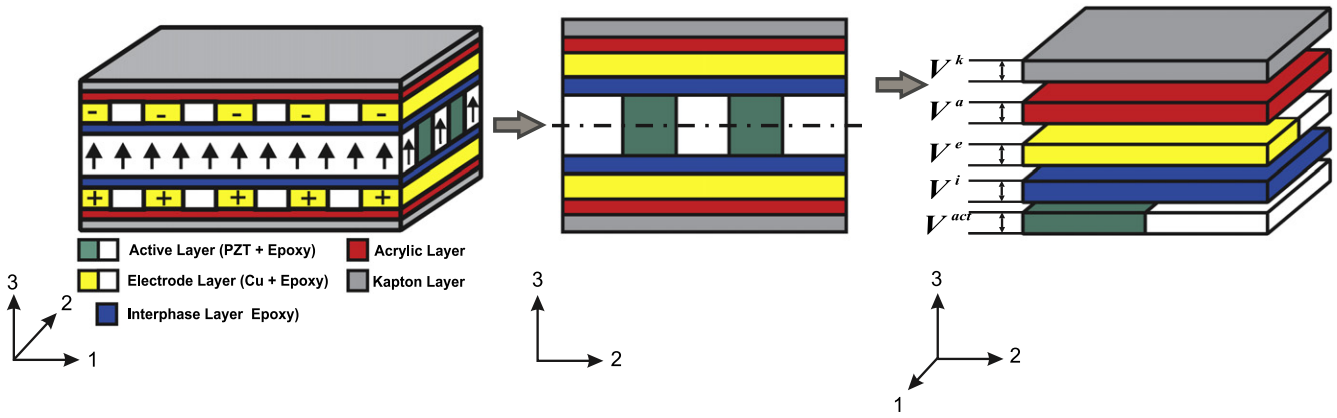

Figure 2. Schematic representation of the d_{31}-type MFC as an equivalent layered model with active, bonding layer, electrode, acrylic, and kapton layers.

Table 2. Assumptions for the homogenization of d_{31}-type MFC using an equivalent layered approach.

Sequence of formulation	Iso-field assumptions $x^c = x^f = x^m$	Weighted average assumptions $x^c = V^f x^f + (1-V^f)\, x^m$
	$x \in (S, T, E, D)$	
Electrode layer (V^e)	S_2, S_3, S_4 T_1, T_5, T_6 E_3	S_1, S_5, S_6 T_2, T_3, T_4 D_3
Homogenized layer (V^{act} & V^i)	S_1, S_2, S_6 T_3, T_4, T_5 D_3	S_3, S_4, S_5 T_1, T_2, T_6 E_3
Homogenized layer (V^{act}, V^i & V^e) (V^{act}, V^i, V^e & V^a) (V^{act}, V^i, V^e, V^a & V^k)	S_1, S_2, S_6 T_3, T_4, T_5	S_3, S_4, S_5 T_1, T_2, T_6 $E_3^c = V^f E_3^f$, $D_3^c = V^f D_3^f$

layer has a significant role for load transfer from matrix to reinforcement [20].

To account for the effect of imperfect contact conditions between fiber and matrix, different analytical and numerical models were reported and unique characteristics between different models were analyzed [21]. Mechanical imperfections between fiber and matrix interface of 1–3 type piezocomposites were modeled using a spring-factor model and the influence of the interface stiffness on the electromechanical load diffusion was examined [22]. A finite element model was developed to study the effect of fiber damage on the performance of AFC and the simulated results indicated a decrease in the effective stiffness resulting from the fiber damage which would lead to the degradation of the AFC actuation performance [23]. Using the complex variable theory and AHM mechanical imperfect contact at the bonding layer was studied via linear spring model by Ramos *et al* [24]. The authors observed, while the overall performance of 1–3 piezocomposite improved due to the normal imperfect contact condition, acoustic impedance of the composite reduced. Thus, the analysis of bonding layer effects has been found critical in studying the behavior of piezocomposites.

In the current work, an attempt is made to evaluate the effective electromechanical properties of d_{31} and d_{33} type MFCs based on equivalent layered approach [25] where all layers (kapton, acrylic, electrode, and active) along with bonding layer are considered for homogenization. Also, a numerical model based on a representative volume element is proposed. The simulated results based on analytical and numerical models are compared with experimental measurements. The outline of the paper is as follows: the analytical model formulation is discussed in section 2 based on the constitutive behavior of MFC and the assumptions for d_{31} and d_{33} type MFCs. Section 3 elaborates the periodic boundary conditions and the calculation of effective properties using RVE which are validated by experiments given in section 4. Aspects of the implementation, analytical treatment and numerical examples are discussed in section 5. Finally, a summary concludes the paper in section 6.

2. Analytical model formulation

MFCs are made up of seven layers, namely, one active layer (PZT fibers embedded in epoxy matrix), two electrode (copper fibers embedded in epoxy matrix), acrylic and kapton layers which are placed on top and bottom of active layer. The bonding layer between active and electrode layer is modeled as a separate layer for homogenization resulting in a nine layered composite in the current work. Based on the design of electrode and the poling direction of fibers, MFCs are categorized as follows: (i) d_{33} mode where the poling direction is parallel to the fiber direction rendering longitudinal strain and (ii) d_{31} mode where the poling direction is perpendicular to the fiber direction which provides transverse strain; refer to figure 1.

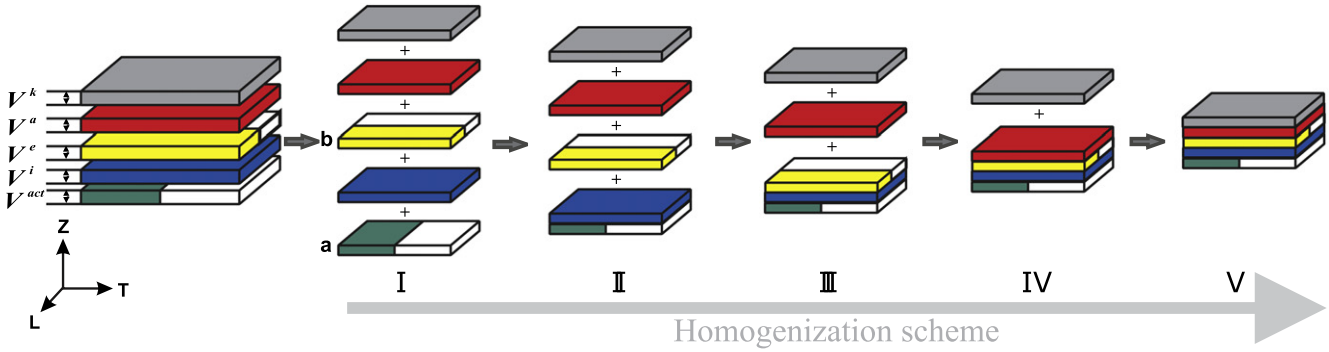

Figure 3. Illustration of homogenization scheme of MFC for analytical formulation.

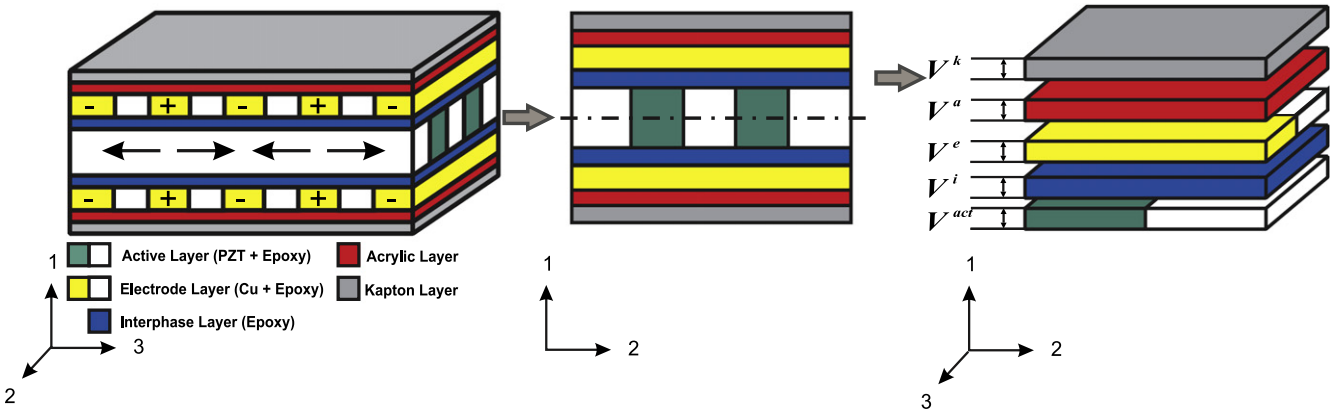

Figure 4. Schematic representation of a d_{33}-type MFC as an equivalent layered model with active, bonding, electrode, acrylic, and kapton layers.

The linear behavior of MFC can be explained by the constitutive equations of piezoelectric materials as follows:

$$S_{ij} = s^{E}_{ijkl} T_{kl} + d_{kij} E_k$$
$$D_i = d_{ikl} T_{kl} + \varepsilon^{T}_{ik} E_k \tag{1}$$

where T_{kl}, S_{ij}, E_k and D_i are the second order stress, stain and first order electric field, electric displacement tensors respectively. s^{E}_{ijkl}, d_{kij} and ε^{T}_{ik} are the fourth order compliance, third order piezoelectric charge and second order permittivity tensors respectively. The superscripts E and T indicate that the compliance and permittivity constants are determined under the conditions of zero or constant electric field and stress. Based on the representation of Nye [26], equation (1) can be restated as:

$$S_m = s^{E}_{mn} T_n + d_{pm} E_p$$
$$D_q = d_{qn} T_n + \varepsilon^{T}_{qp} E_p \tag{2}$$

where the subscript m and n are deduced from ij and kl. For instance, ij or kl = 11, 22, 33, 23, 13 or 12 can be represented as m or n = 1, 2, 3, 4, 5 or 6 (e.g., $s_{1113} = s_{15}$) and for p or q = 1, 2 or 3. Similarly, the stress tensor (n) and the strain tensor (m) can be represented in the compact notation 1, 2, 3, 4, 5, 6 (e.g., $S_{11} = S_1$, $2S_{12} = S_6$). The constitutive behavior of MFC can be written in matrix form (Voigt's notation),

$$\begin{pmatrix} S_1^x \\ S_2^x \\ S_3^x \\ S_4^x \\ S_5^x \\ S_6^x \\ \hline D_1^x \\ D_2^x \\ D_3^x \end{pmatrix} = \left[\begin{array}{cccccc|ccc} s_{11}^x & s_{12}^x & s_{13}^x & 0 & 0 & 0 & 0 & 0 & d_{31}^x \\ s_{12}^x & s_{22}^x & s_{23}^x & 0 & 0 & 0 & 0 & 0 & d_{32}^x \\ s_{13}^x & s_{23}^x & s_{33}^x & 0 & 0 & 0 & 0 & 0 & d_{33}^x \\ 0 & 0 & 0 & s_{44}^x & 0 & 0 & 0 & d_{24}^x & 0 \\ 0 & 0 & 0 & 0 & s_{55}^x & 0 & d_{15}^x & 0 & 0 \\ 0 & 0 & 0 & 0 & 0 & s_{66}^x & 0 & 0 & 0 \\ \hline 0 & 0 & 0 & 0 & d_{15}^x & 0 & \varepsilon_{11}^x & 0 & 0 \\ 0 & 0 & 0 & d_{24}^x & 0 & 0 & 0 & \varepsilon_{22}^x & 0 \\ d_{31}^x & d_{32}^x & d_{33}^x & 0 & 0 & 0 & 0 & 0 & \varepsilon_{33}^x \end{array}\right] \times \begin{pmatrix} T_1^x \\ T_2^x \\ T_3^x \\ T_4^x \\ T_5^x \\ T_6^x \\ \hline E_1^x \\ E_2^x \\ E_3^x \end{pmatrix} \tag{3}$$

where, the superscript x refers to composite as c, fiber as f and matrix as m. For instance, the normal strain in the direction 3 of composite, fiber and matrix can be written in the equation form as,

$$S_3^c = s_{13}^c T_1^c + s_{23}^c T_2^c + s_{33}^c T_3^c + d_{33}^c E_3^c \quad (4)$$

$$S_3^m = s_{13}^m T_1^m + s_{23}^m T_2^m + s_{33}^m T_3^m + d_{33}^m E_3^m \quad (5)$$

$$S_3^f = s_{13}^f T_1^f + s_{23}^f T_2^f + s_{33}^f T_3^f + d_{33}^f E_3^f \quad (6)$$

In the present work, the constitution (superscript representation) of fiber f, matrix m, and homogenized composite c is varied based on the consideration of different layers for homogenization; refer to table 1 and figure 3.

2.1. Calculation of effective properties using an equivalent layered approach

To develop a simple analytical model, the nine layers of the MFC are approximated to five layers: active, electrode, bonding, acrylic, and kapton layers, with appropriate volume fractions for both types of MFCs. For more information, refer to figures 2, 3, and 4 and also to information in the following sections. The proposed analytical model is based on an equivalent layered approach where the second phase layer thickness variation is directly proportional to the volume fraction of individual phases. The assumptions employed in the proposed analytical model are based on the concept of 'the rule of mixtures' and series and parallel capacitance theory [25, 27, 28].

The formulation to evaluate the effective properties of a composite using an equivalent layered approach is as follows:

- Using the assumptions based on the 'rule of mixtures' and the 'series and parallel capacitance theory,' the stress and electric field components of the matrix in equation (5) are replaced as fiber and composite components.
- The relation between fiber and composite components is obtained using the derived equation (5) and equation (6).
- Using the expressions obtained from the previous step and equation (6), the fiber strain field (S_3^f) is expressed as a function of composite components alone.
- Finally, the electromechanical constants are obtained by equating the coefficients in the derived fiber strain field (equation 6) and the composite strain field (equation 4).

The schematic representation of the equivalent layered models of d_{31}- and d_{33}-type MFCs is shown in figures 2 and 4. From these figures, it is evident that the active layers in both types of MFCs have piezoelectric and matrix phases in series connection along direction 2, and parallel along directions 1 and 3. Hence, the assumptions and the evaluated effective properties of the active layer are common for both types of MFCs. The assumptions for the active layer and the derived effective properties are reported in [29].

Table 3. Assumptions for the homogenization of a d_{33}-type MFC using an equivalent layered approach.

Sequence of formulation	Iso-field assumptions $x^c = x^f = x^m$	Weighted average assumptions $x^c = V^f x^f + (1-V^f)\, x^m$
	$x \in (S, T, E, D)$	
Electrode layer (V^e)	S_1, S_2, S_6 T_3, T_4, T_5 E_3	S_3, S_4, S_5 T_1, T_2, T_6 D_3
Homogenized layer (V^{act} & V^i)	S_2, S_3, S_4 T_1, T_5, T_6 D_3	S_1, S_5, S_6 T_2, T_3, T_4 E_3
Homogenized layer (V^{act}, V^i & V^e) (V^{act}, V^i, V^e & V^a) (V^{act}, V^i, V^e, V^a & V^k)	S_2, S_3, S_4 T_1, T_5, T_6 E_3	S_1, S_5, S_6 T_2, T_3, T_4 D_3

2.1.1. d_{31}-type MFC. In general, the equivalent layered approach is used for the homogenization of two different phases at a time. Hence, the analytical model formulation starts with separate homogenization of the active and electrode layers. The next level of homogenization is carried out with the previously homogenized active layer (as fiber) along with the bonding layer (as matrix). Subsequent homogenizations are carried out using the method described in figure 3 and table 1, where V refers the volume fraction and superscript act, i, e, a, and k refer to the active, bonding, electrode, acrylic, and kapton layers, respectively.

The mechanical and electrical assumptions for the homogenization of different layers of d_{31}-type MFC are tabulated in table 2 per the concepts of the 'rule of mixtures' and the 'series and parallel capacitance theory.' The electrode layer, which consists of copper fiber and epoxy matrix, is in parallel with the applied mechanical load along directions 2 and 3. The fiber and matrix are assumed to be perfectly bonded, so when load is applied along directions 2 and 3, both phases will deform equally, resulting in an iso-strain condition. Due to the assumption of perfect load transfer, the applied load along direction 1 will be same for both phases, resulting in an iso-stress condition. Similar arguments are extended for the homogenization of consecutive layers. The electrical assumptions are made by considering each phase as a capacitor that is connected in series or parallel. For the electrode layer, it is assumed that the electric fields (E_3) of composite, fiber, and matrix are equal, whereas in reality the electric field inside a conductor (copper fiber) is zero. The assumption can be justified since the dielectric permittivity of the PZT is very high compared to copper, and because of this, the accumulated electric displacement on the copper rods is negligible. Also, the

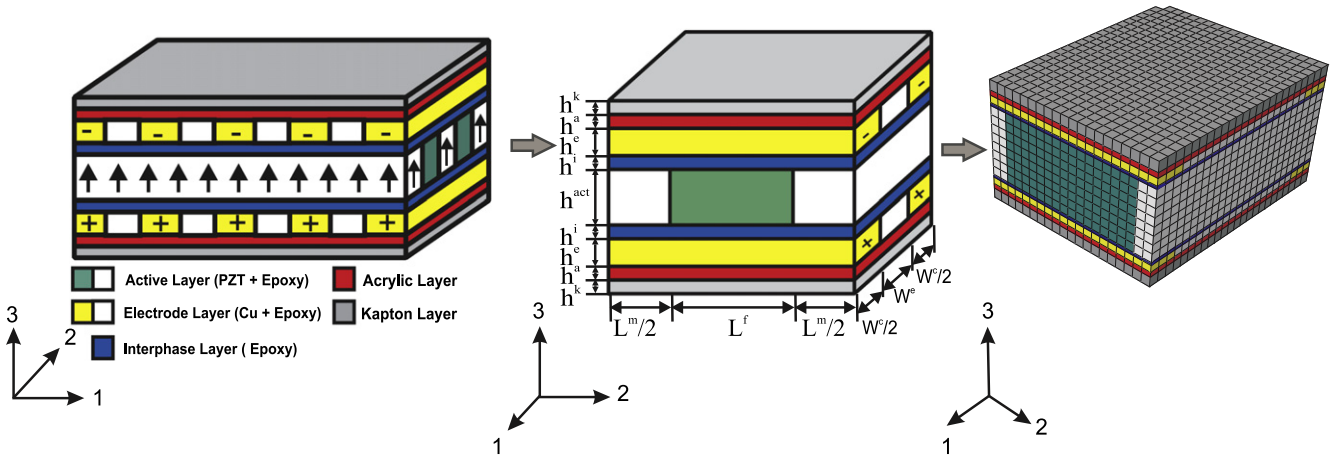

Figure 5. RVE for the d_{31}-type MFC.

bonding layer and active layers are in series connection; therefore, the electric field in direction 3 is weighted with its volume fractions. Due to the electrode configuration in the d_{31}-type MFC, the acrylic and kapton layers are not subjected to the electric field. Hence, during the analytical formulation, the electric field is applied to the active layer alone. The analytical formulation described in section 2.1 is carried out to find the effective properties of the d_{31}-type MFC using the previously mentioned assumptions. The evaluated effective properties for homogenized active and bonding layers are shown as

$$
\begin{aligned}
s_{11}^c &= A_{11}s_{11}^f + A_{21}s_{12}^f + A_{41}d_{31}^f \\
s_{12}^c &= A_{12}s_{11}^f + A_{22}s_{12}^f + A_{42}d_{31}^f \\
s_{13}^c &= A_{13}s_{11}^f + A_{23}s_{12}^f + A_{43}d_{31}^f + s_{13}^f \\
s_{22}^c &= A_{12}s_{12}^f + A_{22}s_{22}^f + A_{42}d_{32}^f \\
s_{23}^c &= A_{13}s_{12}^f + A_{23}s_{22}^f + A_{43}d_{32}^f + s_{23}^f \\
s_{33}^c &= V^f\left(A_{13}\left(s_{13}^f - s_{13}^m\right) + A_{23}\left(s_{23}^f - s_{23}^m\right) + A_{43}\right. \\
&\quad \left.\times\left(d_{33}^f - d_{33}^m\right)\right. \\
&\quad \left. + s_{33}^f\right) + \; d_{33}^f + \left(1 - V^f\right)s_{33}^m \\
s_{44}^c &= V^f s_{44}^f + \left(1 - V^f\right)s_{44}^m \\
s_{55}^c &= V^f s_{55}^f + \left(1 - V^f\right)s_{55}^m \\
s_{66}^c &= s_{66}^f C \\
d_{31}^c &= A_{15}s_{11}^f + A_{25}s_{12}^f + A_{45}d_{31}^f \\
d_{32}^c &= A_{15}s_{12}^f + A_{25}s_{22}^f + A_{45}d_{32}^f \\
d_{33}^c &= V^f\left(A_{15}\left(s_{13}^f - s_{13}^m\right) + A_{25}\left(s_{23}^f - s_{23}^m\right) + A_{45}\right. \\
&\quad \left.\times\left(d_{33}^f - d_{33}^m\right)\right) + d_{33}^f \\
\varepsilon_{33}^c &= V^f\left(A_{15}d_{31}^f + A_{25}d_{32}^f\right) + A_{45}\varepsilon_{33}^f
\end{aligned}
\tag{7}
$$

where the superscript c, f, and m refer to homogenized (active and bonding layer), active, and bonding layers, respectively, as mentioned in sequence II of table 1. Further homogenizations are carried out, and the effective properties of a complete d_{31}-type MFC are as follows:

$$
\begin{aligned}
s_{11}^c &= B_{11}s_{11}^f + B_{21}s_{12}^f \\
s_{12}^c &= B_{12}s_{11}^f + B_{22}s_{12}^f \\
s_{13}^c &= B_{13}s_{11}^f + B_{23}s_{12}^f + s_{13}^f \\
s_{22}^c &= B_{12}s_{12}^f + B_{22}s_{22}^f \\
s_{23}^c &= B_{13}s_{12}^f + B_{23}s_{22}^f + s_{23}^f \\
s_{33}^c &= V^f\left(B_{13}\left(s_{13}^f - s_{13}^m\right) + B_{23}\left(s_{23}^f - s_{23}^m\right) + s_{33}^f\right) \\
&\quad + d_{33}^f + \left(1 - V^f\right)s_{33}^m \\
s_{44}^c &= V^f s_{44}^f + \left(1 - V^f\right)s_{44}^m \\
s_{55}^c &= V^f s_{55}^f + \left(1 - V^f\right)s_{55}^m \\
s_{66}^c &= s_{66}^f C \\
d_{31}^c &= B_{15}s_{11}^f + B_{25}s_{12}^f + d_{31}^f/V^f \\
d_{32}^c &= B_{15}s_{12}^f + B_{25}s_{22}^f + d_{32}^f/V^f \\
d_{33}^c &= V^f\left(B_{15}\left(s_{13}^f - s_{13}^m\right) + B_{25}\left(s_{23}^f - s_{23}^m\right)\right) + d_{33}^f \\
\varepsilon_{33}^c &= B_{15}V^f d_{31}^f + B_{25}V^f d_{32}^f + \varepsilon_{33}^f.
\end{aligned}
\tag{8}
$$

The required constants, A_{ij}, B_{ij}, and C, are listed in appendix A. A detailed explanation of the derived macroscopic effective properties of d_{31}-type MFCs are discussed in section 5.1.

2.1.2. d_{33}-type MFC. As described in section 2.1.1, the equivalent layered approach is also adopted for d_{33}-type MFCs. Here, the electric field generated across the electrodes due to the interdigitated electrode pattern is rather complex when compared with d_{31}-type MFCs. In a simple analytical

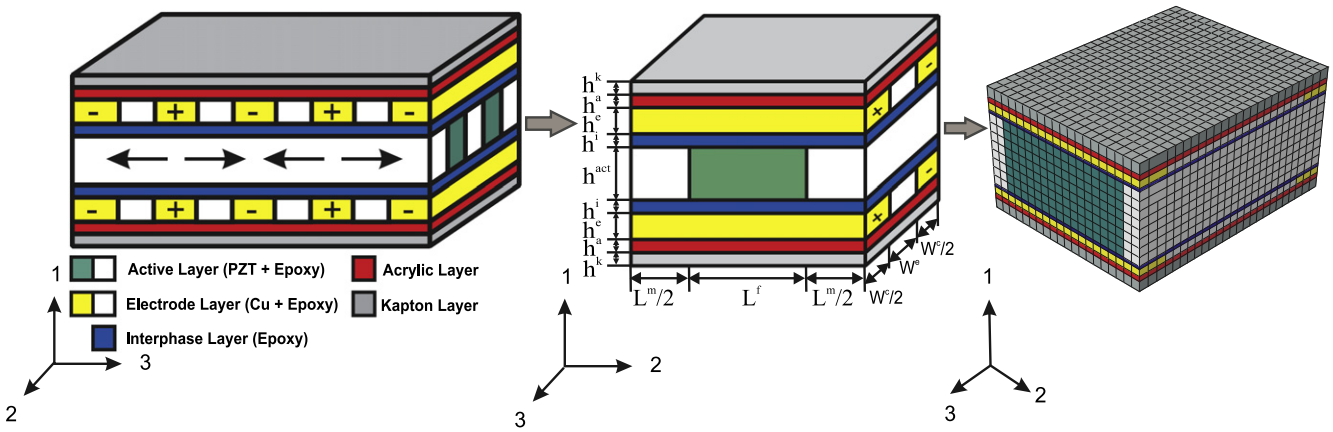

Figure 6. RVE for the d_{33}-type MFC.

model, it would be complex to consider the curved electric field. Hence, a uniform electric field is assumed for analytical formulation. The assumptions for the homogenization of d_{33}-type MFCs are given in table 3.

The evaluated effective properties for the homogenized active and bonding layers of a d_{33}-type MFC are

$$
\begin{aligned}
s_{11}^c &= V^f\left(F_{11}\left(s_{12}^f - s_{12}^m\right) + F_{21}\left(s_{13}^f - s_{13}^m\right)\right.\\
&\quad \left. + F_{41}\left(d_{31}^f - d_{31}^m\right) + s_{11}^f\right) + \left(1 - V^f\right)s_{11}^m\\
s_{12}^c &= V^f\left(F_{12}\left(s_{12}^f - s_{12}^m\right) + F_{22}\left(s_{13}^f - s_{13}^m\right)\right.\\
&\quad \left. + F_{42}\left(d_{31}^f - d_{31}^m\right)\right) + s_{12}^m\\
s_{13}^c &= V^f\left(F_{13}\left(s_{12}^f - s_{12}^m\right) + F_{23}\left(s_{13}^f - s_{13}^m\right)\right.\\
&\quad \left. + F_{43}\left(d_{31}^f - d_{31}^m\right)\right) + s_{13}^m\\
s_{22}^c &= F_{12}s_{22}^f + F_{22}s_{23}^f + F_{42}d_{32}^f\\
s_{23}^c &= F_{13}s_{22}^f + F_{23}s_{23}^f + F_{43}d_{32}^f\\
s_{33}^c &= F_{13}s_{23}^f + F_{23}s_{33}^f + F_{43}d_{33}^f\\
s_{44}^c &= s_{44}^f C\\
s_{55}^c &= V^f s_{55}^f + \left(1 - V^f\right)s_{55}^m\\
s_{66}^c &= V^f s_{66}^f + \left(1 - V^f\right)s_{66}^m\\
d_{31}^c &= V^f\left(F_{15}\left(s_{12}^f - s_{12}^m\right) + F_{25}\left(s_{13}^f - s_{13}^m\right)\right.\\
&\quad \left. + F_{45}\left(d_{31}^f - d_{31}^m\right)\right) + d_{31}^m\\
d_{32}^c &= F_{15}s_{22}^f + F_{25}s_{23}^f + F_{45}d_{32}^f\\
d_{33}^c &= F_{15}s_{23}^f + F_{25}s_{33}^f + F_{45}d_{33}^f\\
\varepsilon_{33}^c &= F_{15}d_{32}^f + F_{25}d_{33}^f + F_{45}\varepsilon_{33}^f
\end{aligned}
\tag{9}
$$

where the superscript c, f, and m refer to homogenized (active and bonding layer), active, and bonding layer, respectively, as mentioned in sequence II of table 1. The effective properties of a homogenized d_{33}-type MFC are

$$
\begin{aligned}
s_{11}^c &= V^f\left(G_{11}\left(s_{12}^f - s_{12}^m\right) + G_{21}\left(s_{13}^f - s_{13}^m\right) + s_{11}^f\right)\\
&\quad + \left(1 - V^f\right)s_{11}^m\\
s_{12}^c &= V^f\left(G_{12}\left(s_{12}^f - s_{12}^m\right) + G_{22}\left(s_{13}^f - s_{13}^m\right)\right) + s_{12}^m\\
s_{13}^c &= V^f\left(G_{13}\left(s_{12}^f - s_{12}^m\right) + G_{23}\left(s_{13}^f - s_{13}^m\right)\right) + s_{13}^m\\
s_{22}^c &= G_{12}s_{22}^f + G_{22}s_{23}^f\\
s_{23}^c &= G_{13}s_{22}^f + G_{23}s_{23}^f\\
s_{33}^c &= G_{13}s_{23}^f + G_{23}s_{33}^f\\
s_{44}^c &= s_{44}^f C\\
s_{55}^c &= V^f s_{55}^f + \left(1 - V^f\right)s_{55}^m\\
s_{66}^c &= V^f s_{66}^f + \left(1 - V^f\right)s_{66}^m\\
d_{31}^c &= V^f\left(G_{15}\left(s_{12}^f - s_{12}^m\right) + G_{25}\left(s_{13}^f - s_{13}^m\right) + d_{31}^f\right)\\
&\quad + \left(1 - V^f\right)d_{31}^m\\
d_{32}^c &= G_{15}s_{22}^f + G_{25}s_{23}^f + d_{32}^f\\
d_{33}^c &= G_{15}s_{23}^f + G_{25}s_{33}^f + d_{33}^f\\
\varepsilon_{33}^c &= V^f\left(G_{15}\left(d_{32}^f - d_{32}^m\right)\right.\\
&\quad \left. + G_{25}\left(d_{33}^f - d_{33}^m\right) + \varepsilon_{33}^f\right) + \left(1 - V^f\right)\varepsilon_{33}^m
\end{aligned}
\tag{10}
$$

where the required constants F_{ij}, G_{ij}, and C can be referred from appendix B. The homogenized effective properties of d_{33}-type MFCs are discussed in section 5.2.

3. Numerical model formulation

The proposed analytical model evaluates the effective properties by considering the volume fraction of constituents alone, while neglecting the effects of the shape (circular or rectangular fiber), orientation, and position of the constituents. Also, an uniform electric field across the electrode is considered in the analytical model, whereas a complex,

Table 4. Boundary conditions for the representative volume element of the MFC.

Cases	Periodic boundary bonditions			
	Electrical	Mechanical		
$1(S_1)$		$u_1^{A+} - u_1^{A-} = k$	$u_2^{B+} - u_2^{B-} = 0$	$u_3^{C+} - u_3^{C-} = 0$
$2(S_2)$		$u_1^{A+} - u_1^{A-} = 0$	$u_2^{B+} - u_2^{B-} = k$	$u_3^{C+} - u_3^{C-} = 0$
$3(S_3)$		$u_1^{A+} - u_1^{A-} = 0$	$u_2^{B+} - u_2^{B-} = 0$	$u_3^{C+} - u_3^{C-} = k$
$4(S_4)$	$\phi^{A+} - \phi^{A-} = 0$	$u_1^{A+} - u_1^{A-} = 0$	$u_3^{B+} - u_3^{B-} = k$	$u_2^{C+} - u_2^{C-} = k$
$5(S_5)$	$\phi^{B+} - \phi^{B-} = 0$	$u_3^{A+} - u_3^{A-} = k$	$u_2^{B+} - u_2^{B-} = 0$	$u_1^{C+} - u_1^{C-} = k$
$6(S_6)$		$u_2^{A+} - u_2^{A-} = k$	$u_1^{B+} - u_1^{B-} = k$	$u_3^{C+} - u_3^{C-} = 0$
$7(E_3)$		$u_1^{A+} - u_1^{A-} = 0$	$u_2^{B+} - u_2^{B-} = 0$	$u_3^{C+} - u_3^{C-} = 0$

nonuniform electric field is generated across the electrodes due to the interdigitated electrode pattern. To account for these issues, a finite-element-based representative volume element (RVE), or unit cell approach [16, 30–32], is used to study the effective properties of the MFC. The schematic representation of the RVE of an MFC is shown in figures 5 and 6.

3.1. Periodic boundary conditions

The composite can be represented by a periodic arrangement of RVEs. To ensure continuous deformation and to avoid overlap between RVEs, periodic boundary conditions are employed. The displacement for an RVE can be written as [33]

$$u_i = S_{ij}^{avg} x_j + u_i^p \tag{11}$$

where S_{ij}^{avg} and u_i^p are average strains and fluctuations in the displacements on boundary surfaces and i, j denote coordinate directions 1, 2, and 3. In a cubic unit cell, the displacements of a pair of opposite boundary surfaces (normal along the x_j axis) can be represented as

$$\begin{aligned} u_i^{S+} &= S_{ij}^{avg} x_j^{S+} + u_i^p, \\ u_i^{S-} &= S_{ij}^{avg} x_j^{S-} + u_i^p \end{aligned} \tag{12}$$

where $S+$ and $S-$ refer to positive and negative x_j directions. For a pair of nodes with the same in-plane coordinates on opposite surfaces, the fluctuation remains same. Therefore, the periodic boundary condition for mechanical loading is represented as

$$u_i^{S+} - u_i^{S-} = S_{ij}^{avg}\left(x_j^{S+} - x_j^{S-}\right). \tag{13}$$

Also, the macroscopic electric field (E) condition can be predicted based on the difference between the electric potential (ϕ) of opposite surfaces as:

$$\phi^{S+} - \phi^{S-} = -E_i^{avg}\left(x_j^{S+} - x_j^{S-}\right). \tag{14}$$

The average mechanical and electrical properties such as stress, strain, electric field, and electric displacement of an RVE are defined using the volume average technique as

$$\begin{aligned} S_{ij}^{avg} &= \frac{1}{vol}\int_{vol} S_{ij}\,dvol \quad \text{and} \quad T_{ij}^{avg} = \frac{1}{vol}\int_{vol} T_{ij}\,dvol \\ E_i^{avg} &= \frac{1}{vol}\int_{vol} E_i\,dvol \quad \text{and} \quad D_i^{avg} = \frac{1}{vol}\int_{vol} D_i\,dvol. \end{aligned} \tag{15}$$

For efficient and fast calculation of homogenized material properties, a PYTHON script is developed in combination with ABAQUS. The macroscopic average fields (strain, stress, electric field, and electric displacement) are calculated using a volume average technique over the total elements as the following

$$\begin{aligned} S_{ij}^{avg} &= \frac{\sum_{e=1}^{N} S_{ij}^e vol^e}{\sum_{e=1}^{N} vol^e} \quad \text{and} \quad T_{ij}^{avg} = \frac{\sum_{e=1}^{N} T_{ij}^e vol^e}{\sum_{e=1}^{N} vol^e} \\ E_i^{avg} &= \frac{\sum_{e=1}^{\overline{N}} E_i^e vol^e}{\sum_{e=1}^{\overline{N}} vol^e} \quad \text{and} \quad D_i^{avg} = \frac{\sum_{e=1}^{\overline{N}} D_i^e vol^e}{\sum_{e=1}^{\overline{N}} vol^e} \end{aligned} \tag{16}$$

where vol, N denotes the volume and the total number of elements in the RVE, and $\overline{N}$ denotes the total number of RVE elements in the active and bonding layers. The superscripts avg and e represent the average value of fields over the RVE and the field values at the element level, respectively. The boundary conditions for the numerical model of the MFC are given in table 4, where k refers to the applied constant deformation and $A+/A-$, $B+/B-$, and $C+$, $C-$ denote the outermost surfaces along directions 1, 2, and 3, respectively.

3.2. Calculation of effective properties using an RVE

For the calculation of elastic constants, the periodic boundary conditions (refer to table 4) are applied in such a way that the displacement is applied along the considered direction, while constraining the displacement in the other directions and maintaining zero potential difference across the electrodes. The average values of the applied strain, induced stress, electric field, and electric displacement are calculated using equation (16). Using the averaged values, effective compliance constants (s_{mn}) are calculated from the linear piezoelectric constitutive relations. Similarly, for the prediction of coupling (d_{mp}) and electrical (ε_{pq}) constants, a voltage difference is applied across the electrodes while constraining the displacement in all directions. Using the constitutive relation and the macroscopic value of applied electric field, induced stress, strain, and electric displacement (using equation (16), the effective properties of MFCs are calculated.

Figure 7(a) shows the induced strain (S_1) for an applied unit voltage difference across the electrodes (E_3; refer to figure 5) and figure 7(b) shows the induced electric displacement (D_3) for an applied unit strain along direction 1.

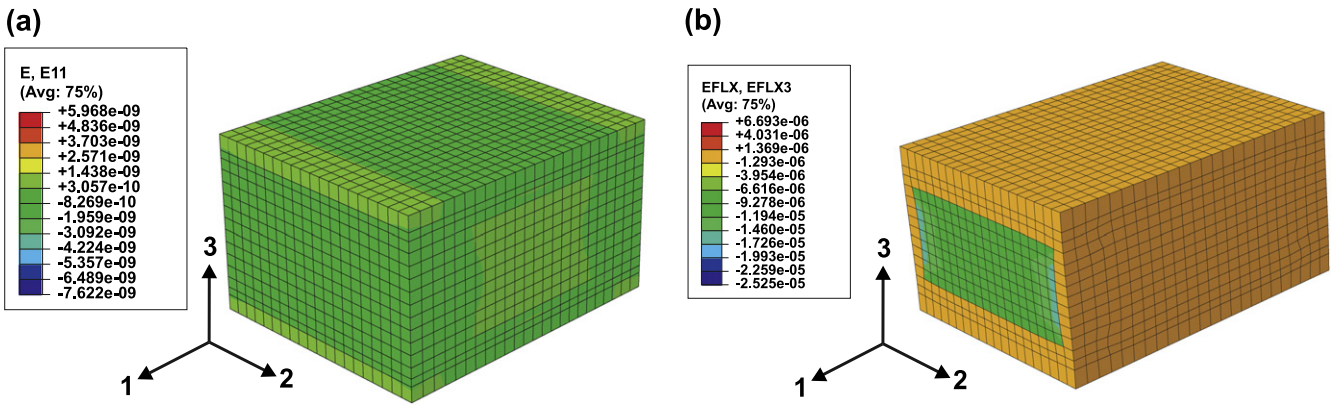

Figure 7. Induced strain (S_1) and electric displacement (D_3) of a d_{31}-type MFC.

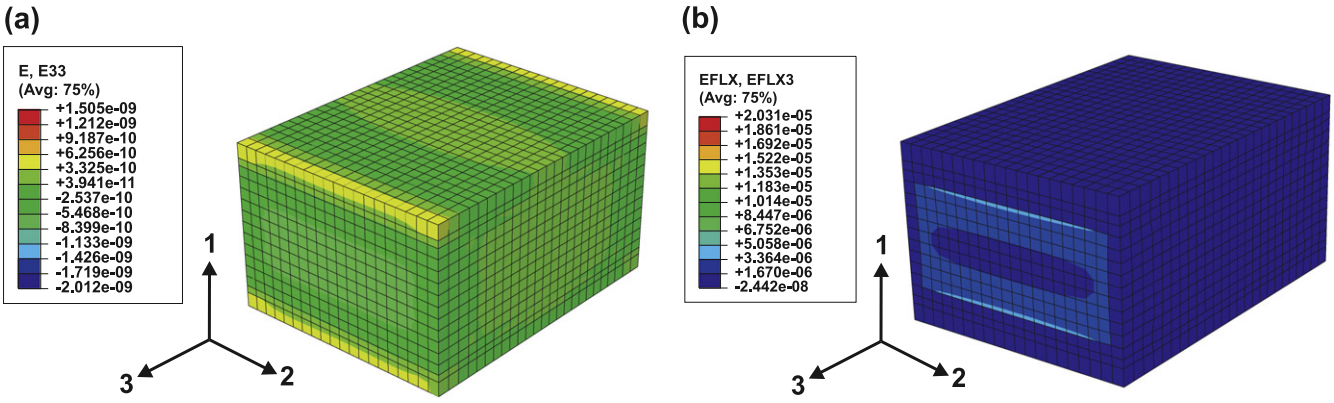

Figure 8. Induced strain (S_3) and electric displacement (D_3) of a d_{33}-type MFC.

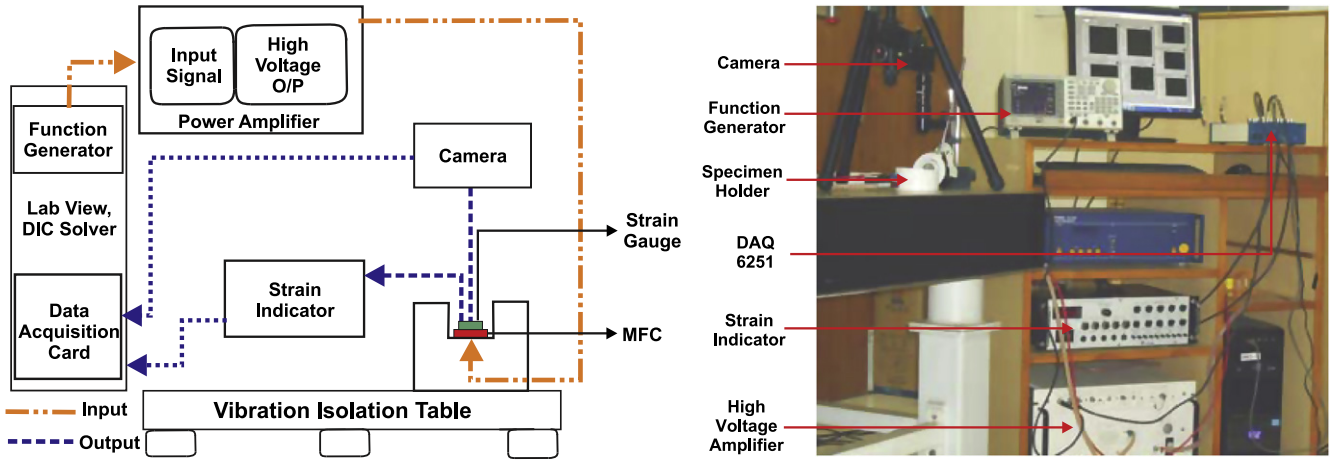

Figure 9. Schematic diagram and photograph of experimental setup.

Figure 8(a) shows the induced strain (S_3) for an applied unit voltage difference across the electrodes(E_3; refer to figure 6) and figure 8(b) shows the induced electric displacement (D_3) for an applied unit strain along direction 3 (sensor).

4. Experimental characterization

Experiments are conducted under pure electrical load to measure the longitudinal strain of MFCs. Figure 9 shows the schematic representation and photograph of the experimental setup.

Through a function generator (Tektronix AFG3022B), a cyclic sinusoidal bipolar wave form is generated and transferred to the voltage amplifier. A high-voltage amplifier (TREK PZD2000A) amplifies the given signal by 200 times; the signal is then used to actuate the MFCs. Using a 90°, two-element cross, plane-type strain gauge (FCB-2–11, A515471, Tokyo Sokki Kenkyujo Co., Ltd.), both the longitudinal and transverse strains of the MFC are measured. The data

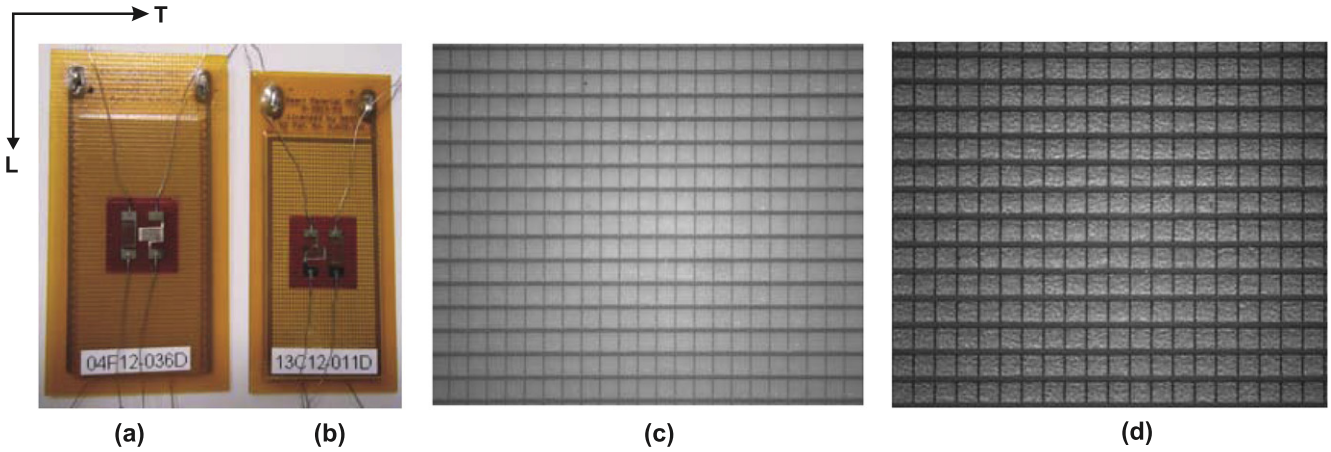

Figure 10. Illustrations of strain gauge positions and directions, along with reference images of both types of MFCs.

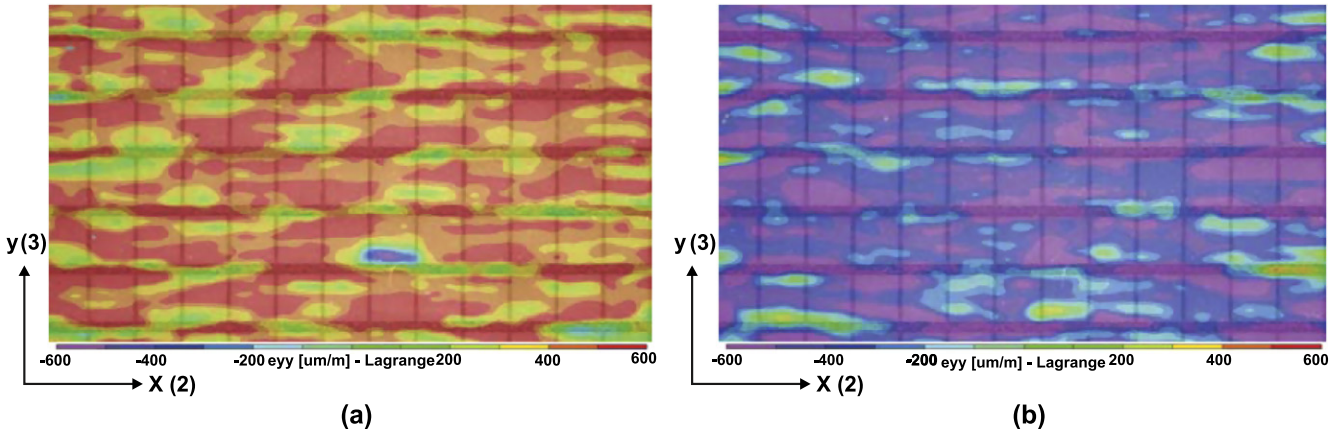

Figure 11. The longitudinal strain field (S_3) of the d_{33}-type MFC.

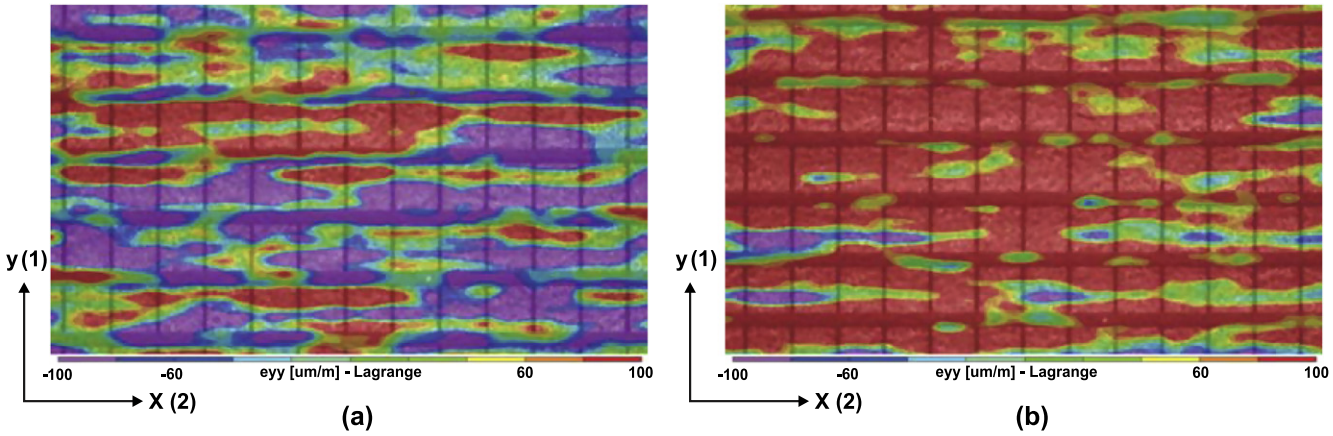

Figure 12. The longitudinal strain field (S_1) of the d_{31}-type MFC.

obtained from the strain gauge are amplified using a strain indicator from SYSCON. The bonding material between the strain gauge and the MFC may influence the obtained results. To study this phenomenon, we use digital image correlation (DIC), a noncontact-type strain measurement technique As both types of MFCs had a sufficient natural speckle pattern to correlate the images, there is no need for external speckling. The images are taken using a camera (GRAS-50S5M-C) with a 6.5X zoom lens (Navitar 1–60123), and the captured images are analyzed in commercially available Vic-2D software. The measured data are recorded on a DAQ card (NI 6251) using Labview. Experiments are performed at room temperature under 'quasi-static' loading conditions. The position of the strain gauge and the directions are shown in figures 10(a) and (b) for d_{33}- and d_{31}-type MFCs, respectively. Figures 10(c) and (d) are the reference images in DIC for the d_{33}- and d_{31}-

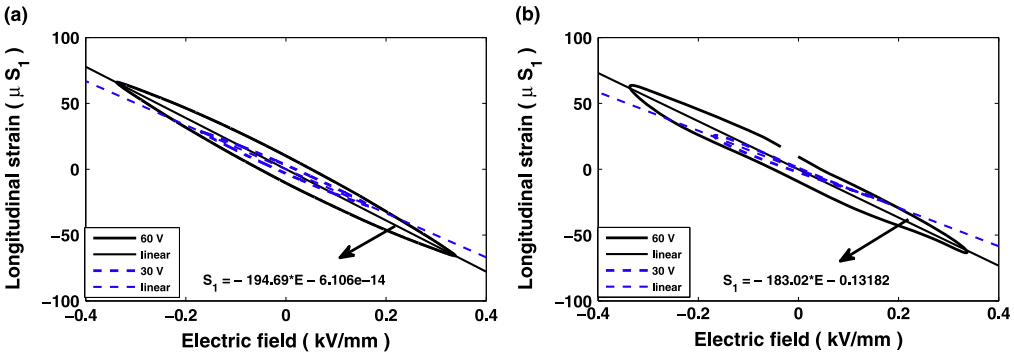

Figure 13. Strain vs. electric field hysteresis behavior of d_{31}-type MFCs.

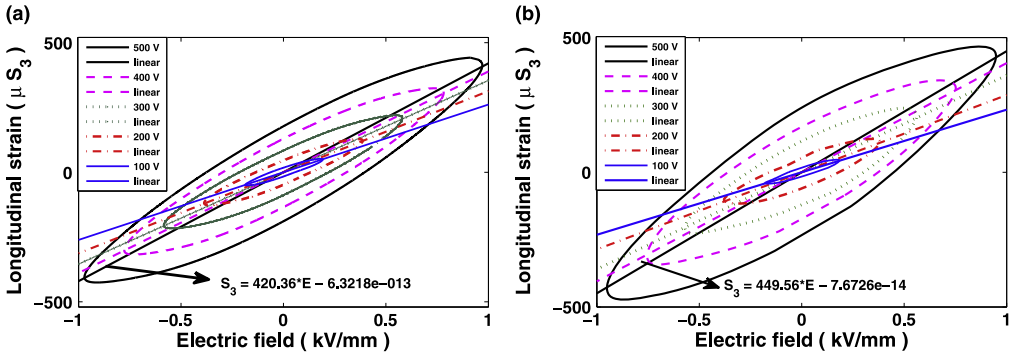

Figure 14. Strain vs. electric field hysteresis behavior of d_{33}-type MFCs.

Table 5. Electric field dependence of the coupling constant of d_{31}-type MFCs.

	d_{31} (pC/N)	
Applied voltage (V)	Strain gauge	DIC
±30	−167.28	−146.21
±60	−194.69	−183.02

Table 6. Electric field dependence of the coupling constant of d_{33}-type MFCs.

	d_{33} (pC/N)	
Applied voltage (V)	Strain gauge	DIC
± 100	261.44	231.9
± 200	312.93	286.4
± 300	354.41	359.6
± 400	388.93	405.11
± 500	420.36	449.56

Table 7. Geometric properties of the MFC laminate [34].

Properties	Values (μ)m
Active layer thickness (h_{act})	177.8
Electrode layer thickness (h_e)	17.78
Acrylic layer thickness (h_a)	12.7
Kapton layer thickness (h_k)	25.4

type MFCs. In the d_{33}-type MFC, the longitudinal strain (S_3) is analyzed by considering the subset size as 29 and the step size as 4. The obtained strain field (S_3) variations are shown in figures 11(a) and (b) where figure 11(a) shows the strain variation for the input of 500 V and figure 11(b) corresponds to the input voltage of −500 V. For the analysis of d_{31}-type MFC the considered subset and step sizes are 37 and 4, respectively. Figures 12(a) and (b) show the longitudinal strain (S_1) distribution of the d_{31}-type MFC for input voltages of 60 V and −60 V, respectively.

The accurate evaluation of the curved electric field that is generated in d_{33}-type MFCs due to the interdigitated electrode is complex. Hence, in the present work, the average electric field is evaluated as [34]

$$E = \frac{V}{w} \tag{17}$$

where V is the applied voltage and w is the center-to-center distance between adjacent interdigitated electrodes.

5. Results and discussion

Experiments are performed under pure electrical load with voltages ranging from ± 100 V to ± 500 V for the d_{33}-(M2814-P1) type MFC and ± 30 V & ± 60 V for the d_{31}-(M2814-P2) type MFC. The variations of strain with the applied electric fields are shown in figures 13 and 14. The effective coupling and electric constants are evaluated using a linear regression analysis; they are tabulated in tables 5 and 6.

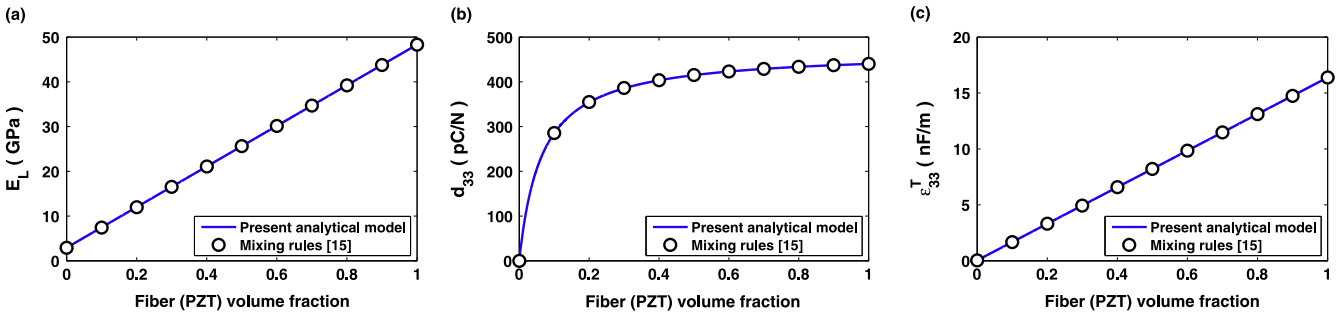

Figure 15. Validation of the proposed analytical model for the active layer, with the mixing rules form the literature [15].

Table 8. MFCs constituent material properties.

Properties	SONOX P502	Epoxy	Copper	Acrylic	Kapton
Young's modulus (GPa)	$\boldsymbol{E_1} = \boldsymbol{E_2} = 54.05$ $\boldsymbol{E_3} = 48.30$	2.9	117.2	2.7	2.5
Shear modulus (GPa)	$G_{23} = G_{13} = 19.48$ $G_{12} = 19.14$	1.11	43.41	1.0	0.93
Poisson's ratio	ν_{23}=ν_{13}= 0.44 $\nu_{12} = 0.41$	0.3	0.35	0.35	0.34
Piezoelectric constants (pC/N)	$d_{31} = d_{32} = -185$ $d_{33} = 440$	—	—	—	—
Dielectric permittivity (nF/m)	$\varepsilon^T_{11} = \varepsilon^T_{22} = 17.2657$ $\varepsilon^T_{33} = 16.3802$	0.0376	0.0443	0.0301	0.0301

It is observed that the coupling constants vary with the applied electric field. A similar behavior is reported in the literature [34] for d_{33}-type MFCs.

To comprehensively understand the effective properties derived from analytical and numerical models, the following geometric (table 7) and material properties (table 8) are considered. The simulated results obtained from analytical and numerical models are compared with the data sheet from Smart Material Corp. (Germany) and with the obtained experimental results. Most of the models (using uniform field method, analytic, and numeric asymptotic homogenization methods) available in the literature were proposed for the active layer. As far as the authors of this paper know, there is no model in the existing literature that accounts for the homogenization of all layers for d_{31}- and d_{33}-type MFCs. Hence, the proposed model is validated with the results of homogenized active layer models (mixing rules [15]). Both mixing rules and equivalent layered approaches are based on the assumptions of the rule of mixture and series and parallel capacitance theory. Hence, the presented results are in line with each other; for more information, refer to figure 15. However, the present analytical model differs from the mixing rule by considering three-dimensional geometric analysis.

Details of the constituent layer thickness in the absence of the bonding layer are given in table 7. The total thickness of the MFC is maintained while considering the bonding layer by varying the thickness of the active, electrode, acrylic, and kapton layers based on appropriate volume fractions. The bonding layer volume fraction is varied (from 0% to 5%) to study its influence on effective properties, whereas the PZT fiber volume fraction in the active layer is maintained, per the Smart Material Corp. standards (86.54%).

5.1. d_{31}-type MFC

MFC samples are observed under a digital microscope (LEICA DFC 295) to measure the width (130 μm) and spacing between the copper rods (360 μm) of the electrode layer. Based on the measurements, the volume fractions of copper and epoxy in the electrode layer are calculated (26.53% of copper and 73.57% of epoxy), and the data are used in numerical formulations. Figure 16 shows the effective mechanical properties of d_{31}-type MFCs as a function of bonding the layer volume fraction. The bonding layer (epoxy) material is relatively soft compared to PZT and copper. Therefore, the effective properties of d_{31}-type MFC decrease gradually as the volume fraction of the bonding layer increases from 0 to 0.05. Figures 16(a)–(c) show the variation of Young's modulus along longitudinal (L), transverse (T), and normal (Z) directions, respectively. It is observed that the reduction in the effective Young's modulus is higher in Z direction compared to directions (L and T). A possible reason could be that, when the load is applied along the direction $1(L)$ and $2(T)$, all the phases are parallel with the applied load. Therefore, the applied load is shared by all the phases. Due to the high stiffness of the PZT and copper, the load

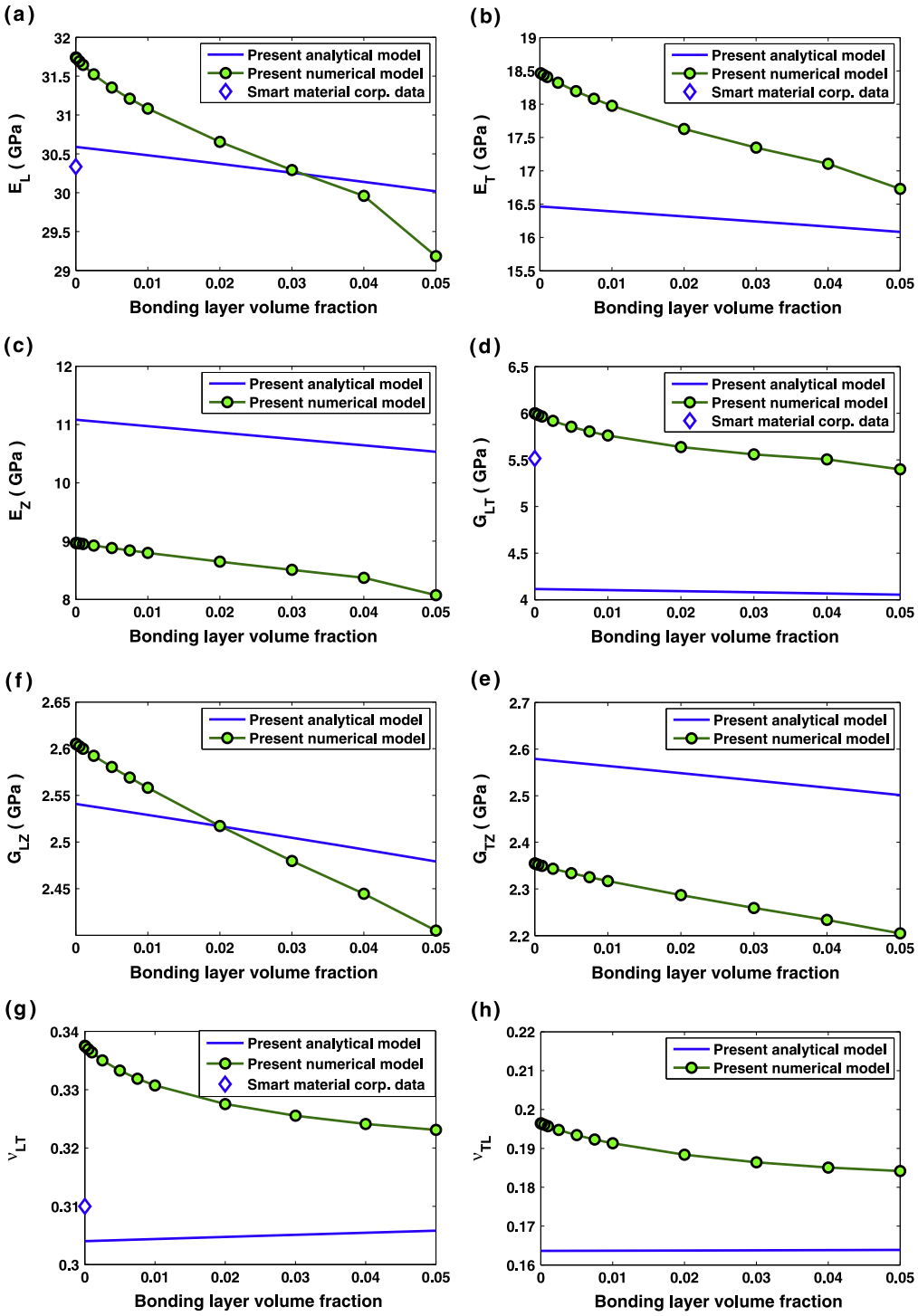

Figure 16. Evolution of effective elastic constants of d_{31}-type MFCs as a function of bonding layer volume fraction.

shared by these fibers is high when compared to other phases, which results in minimal variation the of the Young's modulus with an increase in the bonding layer volume fraction. Similarly, the variation in the shear modulus, G_{LT}, is higher when compared to the shear moduli, G_{LZ} and G_{TZ}. A parametric study is conducted for the predicted effective properties obtained from analytical and numerical models, in which constants (expect for Poisson's ration) show the same behavior, with variation in the bonding layer volume fraction.

The variation of effective coupling (d_{31}, d_{32}, and d_{33}) and electrical (ε_{33}) constants with the bonding layer volume fractions is shown in figure 17. As the electrode layers are placed on top of the bonding layer, the applied electric field has to pass through the bonding layer to the active layer. As the input (electric field) to the MFC is reduced as the volume fraction of the bonding layer is increased, the induced strain, stress, and electric displacement reduce, resulting in a large reduction in coupling and electrical constants even when the

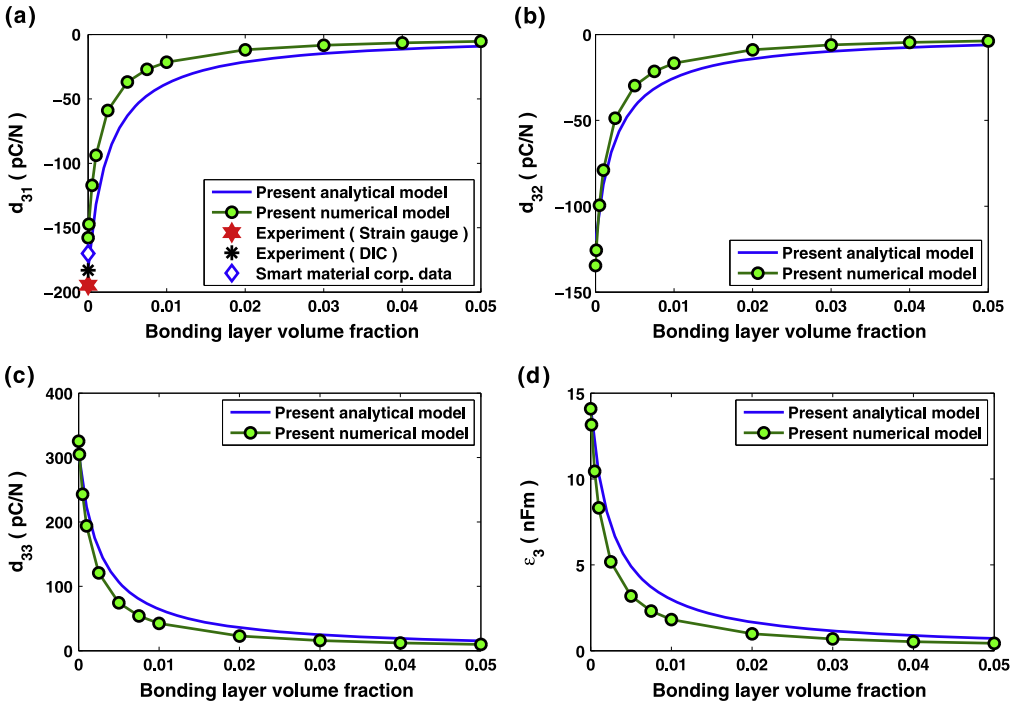

Figure 17. Evolution of effective dielectric and coupling constants of a d_{31}-type MFC as a function of bonding layer volume fraction.

increase in the bonding layer volume fraction is small (0 to 0.03) and remains constant during further increases. This behavior is observed because the dielectric permittivity of the bonding layer material (epoxy, $\varepsilon_{33} = 0.0443$) is substantially lower than PZT ($\varepsilon_{33} = 16.3802$). The predicted results, based on the analytical and numerical models, are in good agreement with each other. Also, some predicted constants are compared with constants obtained through both the experiment and the values available in the data sheet from the manufacturer.

5.2. d_{33}-type MFC

Similarly, the width (137 μ m and spacing between the copper rods (380 μ m are measured for d_{33}-type MFCs and the volume fractions of copper and epoxy in the electrode layer is calculated (26.49% copper and 73.51% epoxy). The variation of effective mechanical properties of d_{33}-type MFCs as a function of the bonding the layer volume fraction is shown in figure 18. Due to the addition of a relatively soft layer as the bonding layer material (epoxy), there is a reduction in the effective properties of d_{33}-type MFCs when compared to MFCs that have no bonding layer. A linear relation between mechanical constants with the variation of the bonding layer volume fraction is observed in most of the effective properties. As stated in section 5.1, due to the high stiffness of PZT and copper (while comparing with the other phases), and also due to the fact that the load is applied in parallel with all phases in the directions L and T, the change in variation of E_L and E_T is smaller with an increase in the bonding layer volume fraction (0 to 5%). Similarly, the reduction in the shear modulus, G_{LT}, is higher the shear modulus in the other directions (G_{TZ} and G_{LZ}).

The electric field distributions along directions 3 in d_{31}- and d_{33}-type MFCs are shown in figures 19(a) and (b). In both figures, the top and bottom three rows of elements correspond to kapton, acrylic, and electrode layers (mechanical layers), respectively. Figure 19(a) clarifies that the electric field distribution in the mechanical layers is less when compared to the active and bonding layers. Hence, the macroscopic values of electric variables from the RVE are calculated in the region of the active and bonding layers; refer to equation (16). However, the electric field distribution in the d_{33}-type MFC (refer to figure 19(b)) shows that the mechanical layers are also subjected to the electric field due to an interdigitated electrode pattern. Hence, the macroscopic values of the electric variables are calculated for full RVE in d_{33}-type MFCs.

Figure 20 illustrates the variation of the coupling (d_{31}, d_{32}, and d_{33}) and electrical (ε_{33}) constants with an increase in the bonding layer volume fraction. As stated in section 5.1, the increase in the bonding layer volume fraction reduces the effective electric field subjected to the active layer. However, due to the interdigitated electrode pattern, an in-plane electric field (curved) is generated across the electrodes, which also results in a decrease in the electric field that is not as rapid as in d_{31}-type MFCs. In an analytical model, a uniform electric field is assumed in which the electric field reduces rapidly as the bonding layer volume fraction increases. This may explain why the predictions of the analytical model deviate from those of the numerical model. Also, the predictions are compared with the experiment and the data available from the manufacturer, which are in good agreement.

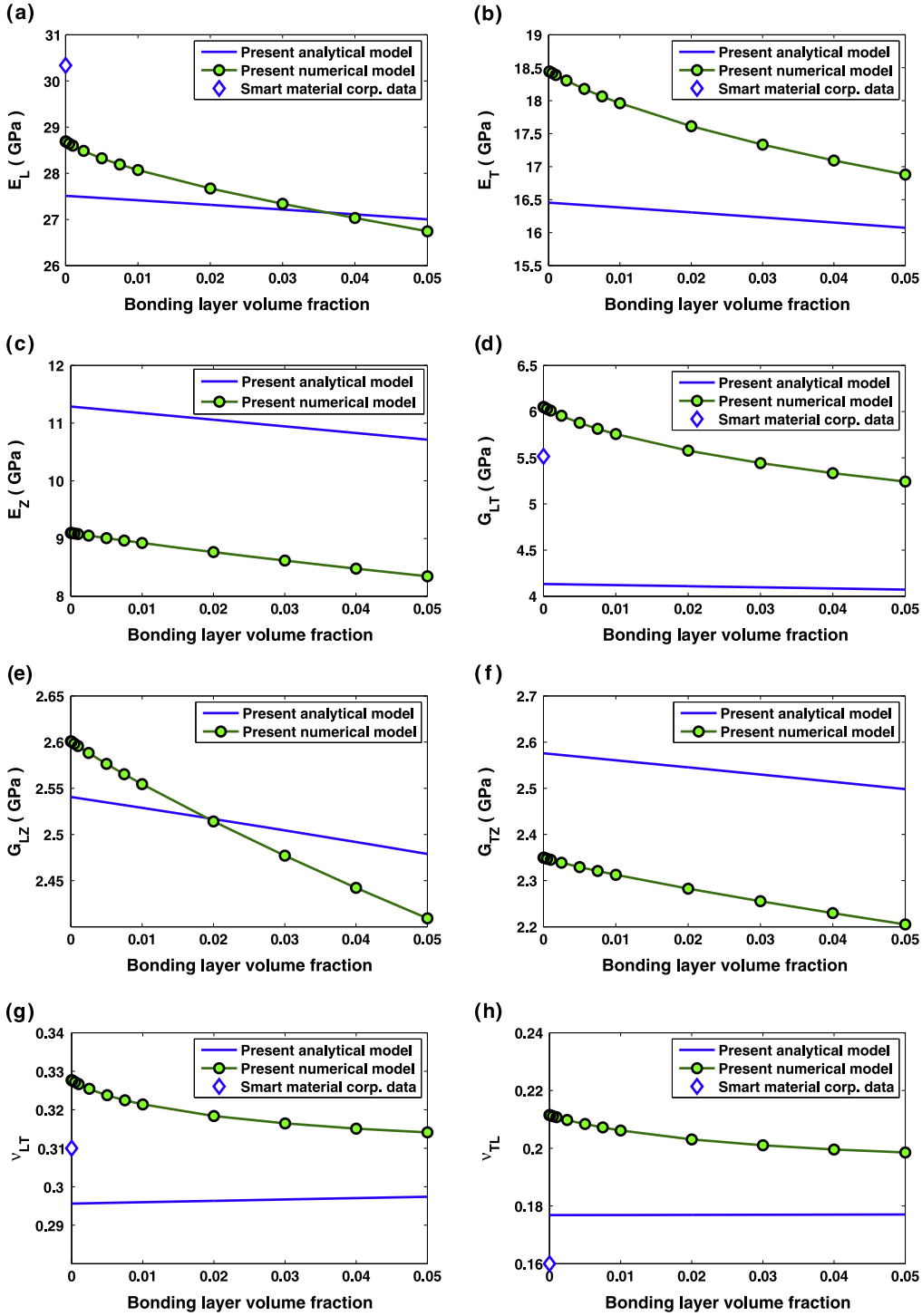

Figure 18. Evolution of effective elastic constants of d_{33}-type MFCs as a function of the bonding layer volume fraction.

6. Summary

In this paper, a simple analytical model (equivalent layered approach) based on the rule of mixtures and the series and parallel capacitance theory was devised to find the effect of the bonding layer on the effective properties of both d_{31}- and d_{33}-type MFCs. The homogenization of the MFC was performed by considering all the layers with appropriate volume fractions. However, geometric properties such as the size, shape, and position of layers and the interdigitated electrode pattern , which also influence the effective properties, were not considered. To account for these parameters, a numerical formulation (FE) using the unit cell approach was proposed with periodic boundary conditions. Experimental measurements were carried out on the MFCs under pure electrical loading to evaluate the effective coupling constants and compare them with the analytical and numerical models and with the data provided from the manufacturer. Using

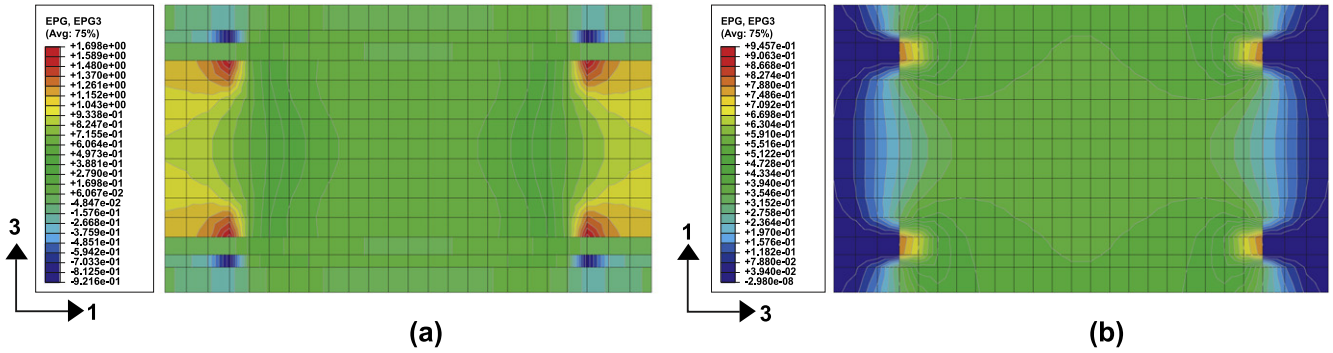

Figure 19. Electric field distribution of d_{31}- and d_{33}-type MFCs along direction 3.

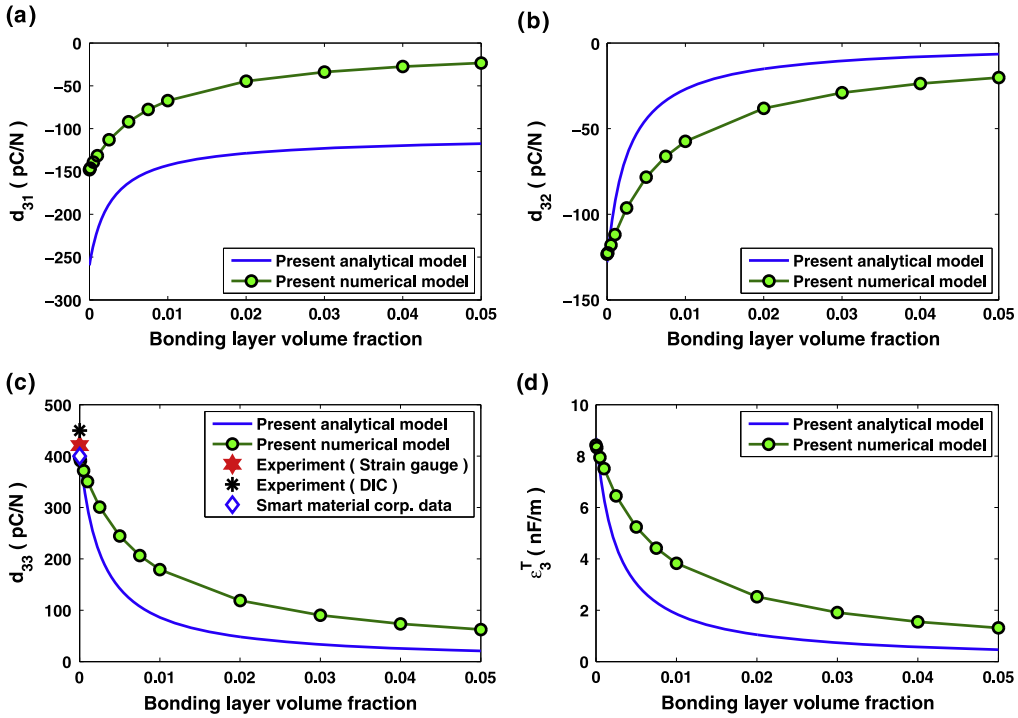

Figure 20. Evolution of the effective dielectric and coupling constants of d_{33}-type MFCs as a function of the bonding layer volume fraction.

analytical and numerical models, a comparative study was carried out to predict the variations of the effective properties with the bonding layer volume fraction. The simulated results show that bonding layer thickness has a significant effect on the coupling and electrical constants, and a comparatively lesser effect on the mechanical constants of both types of MFCs. Because the coupling constants are the unique features of the piezoelectric materials based on the derived electro-mechanical coupling constants, the optimum bonding layer volume fraction is proposed as 0.1% for both d_{31}- and d_{33}-type MFCs.

Acknowledgments

The authors would like to acknowledge financial support from the CSIR—Research scheme (22(0580)/12/EMR-II).

Appendix A

$$A_1 = \left(V^{f2}\left(\varepsilon_{33}^m s_{12}^{mm} - d_{31}^m d_{32}^m\right) + \left(1 - V^f\right)^2\left(\varepsilon_{33}^f s_{12}^f - d_{31}^f d_{32}^f\right) + V^f\left(1 - V^f\right)\left(-d_{31}^f d_{32}^m - d_{31}^m d_{32}^f + \varepsilon_{33}^f s_{12}^{mm} + \varepsilon_{33}^m s_{12}^f\right)\right)$$

$$A_2 = \left(V^{f2}\left(\varepsilon_{33}^m s_{22}^m - d_{32}^{m2}\right) + \left(1 - V^f\right)^2\left(-d_{32}^{f2} + \varepsilon_{33}^f s_{22}^f\right) + V^f\left(1 - V^f\right)\left(-2d_{32}^f d_{32}^m + \varepsilon_{33}^f s_{22}^m + \varepsilon_{33}^m s_{22}^f\right)\right)$$

$$A_3 = \left(V^{f2}\left(d_{32}^m s_{12}^{mm} - d_{31}^m s_{22}^m\right) + \left(1 - V^f\right)^2\left(d_{32}^f s_{12}^f - d_{31}^f s_{22}^f\right) + V^f\left(1 - V^f\right)\left(d_{32}^f s_{12}^{mm} + d_{32}^m s_{12}^f - d_{31}^f s_{22}^m - d_{31}^m s_{22}^f\right)\right)$$

$$A_4 = \left(V^{f2}\left(\varepsilon_{33}^m s_{11}^m V^{f2} - d_{31}^{m2}\right) + \left(1-V^f\right)^2\left(-d_{31}^{f2} + \varepsilon_{33}^f s_{11}^f\right) + V^f\left(1-V^f\right)\left(-2d_{31}^f d_{31}^m + \varepsilon_{33}^f s_{11}^m + \varepsilon_{33}^m s_{11}^f\right)\right)$$

$$A_5 = \left(V^{f2}\left(d_{31}^m s_{12}^{mm} - d_{32}^m s_{11}^m\right) + \left(1-V^f\right)^2\left(d_{31}^f s_{12}^f - d_{32}^f s_{11}^f\right) + V^f\left(1-V^f\right)\left(d_{31}^f s_{12}^{mm} + d_{31}^m s_{12}^f - d_{32}^f s_{11}^m - d_{32}^m s_{11}^f\right)\right)$$

$$A_6 = \left(V^{f2}\left(s_{11}^m s_{22}^m - s_{12}^{m2}\right) + \left(1-V^f\right)^2\left(-s_{12}^{f2} + s_{11}^f s_{22}^f\right) + V^f\left(1-V^f\right)\left(-2s_{12}^f s_{12}^{mm} + s_{11}^f s_{22}^m + s_{11}^m s_{22}^f\right)\right)$$

$$A_7 = \left(1-V^f\right)\left(d_{33}^f - d_{33}^m\right)$$

$$A_8 = \left(1-V^f\right)\left(s_{23}^f - s_{23}^m\right)$$

$$A_9 = \left(1-V^f\right)\left(s_{13}^f - s_{13}^m\right)$$

$$A_{11} = \left(s_{12}^{mm}A_1 - s_{11}^m A_2 - d_{31}^m A_3\right)/A$$

$$A_{12} = \left(s_{22}^m A_1 - s_{12}^{mm}A_2 - d_{32}^m A_3\right)/A$$

$$A_{13} = \left(A_9 A_2 - A_8 A_1 + A_7 A_3\right)/A$$

$$A_{15} = \left(d_{32}^m A_1 - d_{31}^m A_2 - \varepsilon_{33}^m A_3\right)/A$$

$$A_{21} = \left(s_{11}^m A_1 - s_{12}^{mm}A_4 - d_{31}^m A_5\right)/A$$

$$A_{22} = \left(s_{12}^{mm}A_1 - s_{22}^m A_4 - d_{32}^m A_5\right)/A$$

$$A_{23} = \left(A_8 A_4 - A_9 A_1 + A_7 A_5\right)/A$$

$$A_{25} = \left(d_{31}^m A_1 - d_{32}^m A_4 - \varepsilon_{33}^m A_5\right)/A$$

$$A_{34} = s_{66}^m \Big/ \left(s_{66}^f\left(1-V^f\right) + s_{66}^m V^f\right)$$

$$A_{41} = -\left(s_{12}^{mm}A_5 - s_{11}^m A_3 - d_{31}^m A_6\right)/A$$

$$A_{42} = -\left(s_{22}^m A_5 - s_{12}^{mm}A_3 - d_{32}^m A_6\right)/A$$

$$A_{43} = \left(A_7 A_6 + A_8 A_5 + A_9 A_3\right)/A$$

$$A_{45} = -\left(d_{32}^m A_5 - d_{31}^m A_3 - \varepsilon_{33}^m A_6\right)/A$$

$$A = f\left(V^f, \left(1-V^f\right), s_{11}^f, s_{12}^f, s_{22}^f, d_{31}^f, d_{32}^f, \varepsilon_{33}^f, s_{11}^m, s_{12}^m, s_{22}^m, d_{31}^m, d_{32}^m \& \varepsilon_{33}^m\right)$$

$$B_1 = V^f s_{22}^m + \left(1-V^f\right)s_{22}^f$$

$$B_2 = V^f s_{12}^m + \left(1-V^f\right)s_{12}^f$$

$$B_3 = \left(1-V^f\right)\left(s_{23}^f - s_{23}^m\right)$$

$$B_4 = \left(1-V^f\right)\left(s_{13}^f - s_{13}^m\right)$$

$$B_5 = \left(1-V^f\right)\left(d_{32}^f\right)$$

$$B_6 = \left(1-V^f\right)\left(d_{31}^f\right)$$

$$B_7 = V^f s_{11}^m + \left(1-V^f\right)s_{11}^f$$

$$C = s_{66}^m \Big/ \left(V^f s_{66}^m + \left(1-V^f\right)s_{66}^f\right)$$

$$B_{11} = \left(B_1 s_{11}^m - B_2 s_{12}^m\right)/B$$

$$B_{12} = \left(B_1 s_{12}^m - B_2 s_{22}^m\right)/B$$

$$B_{13} = \left(B_2 B_3 - B_1 B_4\right)/B$$

$$B_{15} = \left(B_5 B_2 - B_6 B_1\right)\Big/\left(V^f F\right)$$

$$B_{21} = \left(B_7 s_{12}^m - B_2 s_{11}^m\right)/B$$

$$B_{22} = \left(B_7 s_{22}^m - B_2 s_{12}^m\right)/B$$

$$B_{23} = \left(B_2 B_4 - B_7 B_3\right)/B$$

$$B_{25} = \left(B_6 B_2 - B_5 B_7\right)\Big/\left(V^f F\right)$$

$$B = V^{f2}\left(s_{11}^m s_{22}^m - s_{12}^{m2}\right) + \left(1-V^f\right)^2\left(s_{11}^f s_{22}^f - s_{12}^{f2}\right) + V^f\left(1-V^f\right)\left(s_{11}^m s_{22}^f + s_{11}^f s_{22}^m - 2s_{12}^f s_{12}^m\right)$$

Appendix B

$$F_1 = \left(1-V^f\right)\left(s_{12}^f - s_{12}^m\right)$$

$$F_2 = \left(\varepsilon_{33}^m s_{33}^m V^{f2} + \left(1-V^f\right)^2\left(-d_{33}^{f2} + \varepsilon_{33}^f s_{33}^f\right) + V^f\left(1-V^f\right)\left(\varepsilon_{33}^f s_{33}^m + \varepsilon_{33}^m s_{33}^f\right)\right)$$

$$F_3 = \left(1-V^f\right)\left(s_{13}^f - s_{13}^m\right)$$

$$F_4 = \left(\varepsilon_{33}^m s_{23}^m V^{f2} + \left(1-V^f\right)^2\left(\varepsilon_{33}^f s_{23}^f - d_{32}^f d_{33}^f\right) + V^f\left(1-V^f\right)\left(\varepsilon_{33}^f s_{23}^m + \varepsilon_{33}^m s_{23}^f\right)\right)$$

$$F_5 = \left(V^f\left(d_{33}^f s_{23}^m - d_{32}^f s_{33}^m\right) + \left(1-V^f\right)\left(d_{33}^f s_{23}^f - d_{32}^f s_{33}^f\right)\right)$$

$$F_6 = \left(\varepsilon_{33}^m s_{22}^m V^{f2} + \left(1-V^f\right)^2\left(-d_{32}^{f2} + \varepsilon_{33}^f s_{22}^f\right) + \left(\varepsilon_{33}^f s_{22}^m + \varepsilon_{33}^m s_{22}^f\right)\right)$$

$$F_7 = \left(V^f\left(d_{32}^f s_{23}^m - d_{33}^f s_{22}^m\right) + \left(1-V^f\right)\left(d_{32}^f s_{23}^f - d_{33}^f s_{22}^f\right)\right)$$

$$F_8 = \left(V^{f2}\left(s_{22}^m s_{33}^m - s_{23}^{m2}\right) + \left(1-V^f\right)^2\left(-s_{23}^{f2} + s_{22}^f s_{33}^f\right) + V^f\left(1-V^f\right)\left(s_{22}^f s_{33}^m + s_{22}^m s_{33}^f - 2s_{23}^f s_{23}^m\right)\right)$$

$$C = s_{44}^m \Big/ \left(V^f s_{44}^m + \left(1-V^f\right)s_{44}^f\right)$$

$$F_{11} = \left(F_1 F_2 - F_3 F_4 + \left(1-V^f\right)^2 G5 d_{13}^f\right)\Big/F$$

$$F_{12} = \left(F_4 s_{23}^m - F_2 s_{22}^m\right)/F$$

$$F_{13} = \left(F_4 s_{33}^m - F_2 s_{23}^m\right)/F$$

$$F_{15} = \left(-\left(1-V^f\right)G5\varepsilon_{33}^m\right)\Big/F$$

$$F_{21} = \left(F_3 F_6 - F_1 F_4 + \left(1-V^f\right)^2 G7 d_{13}^f\right)\Big/F$$

$$F_{22} = \left(F_4 s_{22}^m - F_6 s_{23}^m\right)/F$$

$$F_{23} = \left(F_4 s_{23}^m - F_6 s_{33}^m\right)/F$$

$$F_{25} = \left(-\left(1-V^f\right)G7\varepsilon_{33}^m\right)\Big/F$$

$$F_{41} = \left(1 - V^f\right)\left(G3G7 + G1G5 + G8d_{13}^f\right)/F$$
$$F_{42} = -\left(1 - V^f\right)\left(F_7 s_{33}^m + F_5 s_{23}^m\right)/F$$
$$F_{43} = -\left(1 - V^f\right)\left(F_7 s_{23}^m + F_5 s_{22}^m\right)/F$$
$$F_{45} = -\left(G8\varepsilon_{33}^m\right)/F$$
$$F = f\left(V^f, \left(1 - V^f\right), s_{22}^f, s_{23}^f, s_{33}^f, d_{32}^f, d_{33}^f, \varepsilon_{33}^f, s_{22}^m, s_{23}^m, s_{33}^m, d_{32}^m \& \varepsilon_{33}^m\right)$$

$$G_1 = V^f s_{23}^m + \left(1 - V^f\right)s_{23}^f$$
$$G_2 = \left(1 - V^f\right)\left(s_{13}^f - s_{13}^m\right)$$
$$G_3 = V^f s_{33}^m + \left(1 - V^f\right)s_{33}^f$$
$$G_4 = \left(1 - V^f\right)\left(s_{12}^f - s_{12}^m\right)$$
$$G_5 = \left(1 - V^f\right)\left(d_{33}^f - d_{33}^m\right)$$
$$G_6 = \left(1 - V^f\right)\left(d_{32}^f - d_{32}^m\right)$$
$$G_7 = V^f s_{22}^m + \left(1 - V^f\right)s_{22}^f$$
$$C = s_{44}^m\Big/\left(V^f s_{44}^m + \left(1 - V^f\right)s_{44}^f\right)$$
$$G_{11} = \left(G_1 G_2 - G_3 G_4\right)/G$$
$$G_{12} = \left(G_3 s_{22}^m - G_1 s_{23}^m\right)/G$$
$$G_{13} = \left(G_3 s_{23}^m - G_1 s_{33}^m\right)/G$$
$$G_{15} = \left(G_5 G_1 - G_6 G_3\right)/G$$
$$G_{21} = \left(G_1 G_4 - G_7 G_2\right)/G$$
$$G_{22} = \left(G_7 s_{23}^m - G_1 s_{22}^m\right)/G$$
$$G_{23} = \left(G_7 s_{33}^m - G_1 s_{23}^m\right)/G$$
$$G_{25} = \left(G_6 G_1 - G_5 G_7\right)/G$$
$$G = V^{f^2}\left(s_{22}^m s_{33}^m - s_{23}^{m2}\right) + \left(1 - V^f\right)^2\left(s_{22}^f s_{33}^f - s_{23}^{f^2}\right) + V^f\left(1 - V^f\right)\left(s_{22}^m s_{33}^f + s_{22}^f s_{33}^m - 2s_{23}^f s_{23}^m\right)$$

References

[1] Smith R C 2005 Smart material systems—Model development (Philadelphia: SIAM)

[2] Kumar D N, Raja S and Ikeda T 2007 Active vibration control of smart plates with partially debonded multilayered PZT actuators *Smart Mat. Struct.* **194** 1584–94

[3] Betts D N, Kim H A, Bowen C R and Inman D J 2012 Optimal configurations of bistable piezo-composites for energy harvesting *Appl. Phys. Lett* **100** 114104

[4] Konka H P, Wahab M A and Lian K 2013 Piezoelectric fiber composite transducers for health monitoring in composite structures *Sens. Actuators A-Phys* **194** 84–94

[5] Nelson L J 2002 Smart piezoelectric fibre composites *Mater. Sci. Tech* **18** 1245–56

[6] Topolov V Y and Bowen C R 2009 Electromechanical properties in composites based on ferroelectrics (London: Springer)

[7] Bent A A 1997 Active fiber composites structural actuation *PhD thesis, MIT*

[8] Hagood N W, Kindel R, Ghandi K and Gaudenzi P 1993 Improving transverse actuation of piezoceramics using interdigitated surface electrodes. Proc SPIE 1917, Smart Structures and Materials Albuquerque, New Mexico. 1917:341352

[9] Bent A A and Hagood N W 1997 Piezoelectric fiber composites with interdigitated electrodes *J. Intell. Mat. Sys. Struct* **11** 903–19

[10] Wilkie W K, Bryant G R, High J W, Fox R L, Hellbaum R F, Jalink A, Little B D and Mirick P H 2000 Low-cost piezocomposite actuator for structural control applications *Proc. SPIE 7th Annu. Int. Symp. Smart Struct. Mater.* 3991 (CA: Newport Beach) pp 323–34

[11] High J and Wilkie W 2003 Method of fabricating NASA-standard macro-fiber composite piezoelectric actuators NASA/TM-2003-212427 ARL-TR-2833

[12] Park J-S and Kim J-H 2005 Analytical development of single crystal Macro Fiber Composite actuators for active twist rotor blades *Smart Mat. Struct.* **14** 745–53

[13] Raja S and Ikeda T 2007 Concept and electro-elastic modeling of shear actuated fiber composite using micro-mechanics approach *J. Intell. Mater. Syst. Struct* **19** 1173–83

[14] Trindade M A and Benjeddou A 2011 Finite element homogenization technique for the characterization of d 15 shear piezoelectric macro-fibre composites *Smart Mater. Struct.* **20** 075012

[15] Deraemaeker A, Nasser H, Benjeddou A and Preumont A 2009 Mixing rules for the piezoelectric properties of Macro Fiber Composites *J. Intell. Mat. Sys. Struct* **20** 1475–82

[16] Deraemaeker A and Nasser H 2010 Numerical evaluation of the equivalent properties of macro fiber composite (MFC) transducers using periodic homogenization *Int. J. Solids Struct.* **47** 3272–85

[17] Biscani F, Nasser H, Belouettar S and Carrera E 2011 Equivalent electro-elastic properties of Macro Fiber Composite (MFC) transducers using asymptotic expansion approach *Compos.* B **42** 444–55

[18] Biscani F, Nasser H and Belouettar S 2012 Directional dependence of the static response of layered piezoelectric transducers *J. Intell. Mater. Syst. Struct* **23** 1311–22

[19] Kari S, Berger H, Gabbert U, Guinovart-Diaz R, Bravo-Castillero J and Rodriguez-Ramos R 2008 Evaluation of influence of bonding layer material parameters on effective material properties of three phase composites *Compos. Sci. Technol* **68** 684–91

[20] Kuo H-Y 2013 Effective property of multiferroic fibrous composites with imperfect interfaces *Smart Mater. Struct.* **22** 105005

[21] Rodrguez-Ramos R, de Medeiros R, Guinovart-Daz R, Bravo-Castillero J, Otero J A and Tita V 2013 Different approaches for calculating the effective elastic properties in composite materials under imperfect contact adherence *Compos. Struct.* **99** 264–75

[22] Sapsathiarn Y, Senjuntichai T and Rajapakse R K N D 2008 Electro-mechanical load transfer from a fiber in a 1-3 piezocomposite with an imperfect interface, Compos *Part B Eng* **39** 1114–24

[23] Martinez M, Kernaghan R and Artemev A 2009 Finite element analysis of broken fiber effects on hollow active fiber composites *J. Intell. Mater. Syst. Struct* **21** 107–13

[24] Rodrguez-Ramos R, Guinovart-Daz R, Lpez-Realpozo J, Bravo-Castillero J, Otero J A, Sabina F J and Lebon F 2013 Effective properties of periodic fibrous electro-elastic composites with mechanic imperfect contact condition *Int. J. Mech. Sci.* **73** 1–13

[25] Sakthivel M and Arockiarajan A 2012 Thermo-electro-mechanical response of 1-3-2 piezoelectric composites: effect of fiber orientations *Acta Mech.* **223** 1353–69

[26] Nye J F 1985 *Physical properties of crystals* (Oxford: Clarendon)
[27] Tan P and Tong L 2006 Micro-electromechanics models for piezoelectric-fiber-reinforced composite materials *Compos. Sci. Technol* **61** 759–69
[28] Kar-Gupta R and Venkatesh T A 2007 Electromechanical response of 13 piezoelectric composites: A numerical model to assess the effects of fiber distribution *Acta Mater.* **55** 1275–92
[29] Sreenivasa Prasath S and Arockiarajan A 2013 Effective electromechanical response of macro-fiber composite (MFC): Analytical and numerical models *Int. J. Mech. Sci.* **77** 98–106
[30] Xia Z, Zhang Y and Ellyin F 2003 A unified periodical boundary conditions for representative volume elements of composites and applications *Int. J. Solids Struct.* **40** 1907–21
[31] Berger H, Kari S, Gabbert U, Ramos R R, Guinovart R, Otero J A and Castillero J B 2005 An analytical and numerical approach for calculating effective material coefficients of piezoelectric fiber composites *Int. J. Solids Struct.* **42** 5692–714
[32] Berger H, Kari S, Gabbert U, Rodriguez-Ramos R, Bravo-Castillero J, Guinovart-Diaz R, Sabina F J and Maugin G A 2006 Unit cell models of piezoelectric fiber composites for numerical and analytical calculation of effective properties *Smart Mater. Struct.* **15** 451–8
[33] Suquet P 1987 Elements of homogenization theory for inelastic solid mechanics (*Homogenization techniques for composite media*) ed E Sanchez-Palencia and A Zaoui (Berlin: Springer-Verlag)
[34] Williams R B 2004 Non-linear mechanical and actuation characterization of piezoceramic fiber composites *PhD Thesis* (USA: Blacksburg VA)